Sensitivity of Sudden Stratospheric Warmings to Previous Stratospheric Conditions

ALVARO DE LA CÁMARA

National Center for Atmospheric Research, Boulder, Colorado

JOHN R. ALBERS

Cooperative Institute for Research in Environmental Sciences, University of Colorado Boulder, and Physical Sciences Division, NOAA/Earth System Research Laboratory, Boulder, Colorado

THOMAS BIRNER

Department of Atmospheric Science, Colorado State University, Fort Collins, Colorado

ROLANDO R. GARCIA, PETER HITCHCOCK, DOUGLAS E. KINNISON, AND ANNE K. SMITH

National Center for Atmospheric Research, Boulder, Colorado

(Manuscript received 26 April 2017, in final form 14 June 2017)

ABSTRACT

The Whole Atmosphere Community Climate Model, version 4 (WACCM4), is used to investigate the influence of stratospheric conditions on the development of sudden stratospheric warmings (SSWs). To this end, targeted experiments are performed on selected modeled SSW events. Specifically, the model is reinitialized three weeks before a given SSW, relaxing the surface fluxes, winds, and temperature below 10 km to the corresponding fields from the free-running simulation. Hence, the tropospheric wave evolution is unaltered across the targeted experiments, but the stratosphere itself can evolve freely. The stratospheric zonal-mean state is then altered 21 days prior to the selected SSWs and rerun with an ensemble of different initial conditions. It is found that a given tropospheric evolution concomitant with the development of an SSW does not uniquely determine the occurrence of an event and that the stratospheric conditions are relevant to the subsequent evolution of the stratospheric flow toward an SSW, even for a fixed tropospheric evolution. It is also shown that interpreting the meridional heat flux at 100 hPa as a proxy of the tropospheric injection of wave activity into the stratosphere should be regarded with caution and that stratospheric dynamics critically influence the heat flux at that altitude.

1. Introduction

Twice every three years on average, the strong cyclonic polar vortex that dominates the wintertime stratospheric circulation in the extratropical Northern Hemisphere is subject to one of the most impressive dynamical events in the climate system: the so-called sudden stratospheric warming (SSW) (Butler et al. 2015). During an SSW, the vortex is severely displaced off the pole (i.e., a ''displacement'' event) or split into two smaller vortices (i.e., a ''split'' event) in a matter of a few days. Driven by enhanced planetary wave activity, polar temperatures in the stratosphere increase several tens of degrees, and the direction of the zonal-mean winds reverses from westerly to easterly (e.g., Limpasuvan et al. 2004; Charlton and Polvani 2007).

The effects of SSW events are not limited to the polar stratosphere, where they strongly impact the transport and polar processing of chemical constituents (e.g., Manney et al. 2015); the strong circulation disruption caused by SSWs also influences the response of the mesosphere to particle precipitation (e.g., Holt et al. 2013), tropical stratospheric temperatures (e.g., Gómez-Escolar et al. 2014), and tropical upper-tropospheric intrusions of stratospheric air (e.g., Albers et al. 2016). Temperature and wind anomalies during these events descend from the stratosphere to the upper troposphere, where they induce changes in the storm tracks and

Corresponding author: Alvaro de la Cámara, acamara@ucar.edu

DOI: 10.1175/JAS-D-17-0136.1

impact surface weather for up to 2 months (Baldwin and Dunkerton 2001; Thompson et al. 2002; Kolstad et al. 2015; Hitchcock and Simpson 2016). Indeed, seasonal forecast systems have started exploring the enhanced prediction skill in Europe and eastern North America provided by this connection (Marshall and Scaife 2010; Sigmond et al. 2013; Tripathi et al. 2015; Scaife et al. 2016).

Our current understanding of the mechanism of SSWs goes back to Matsuno (1971), who proposed that sudden warmings are dynamical in origin and initiated by the interaction of vertically propagating planetary waves and the stratospheric mean flow. If the waves are sufficiently intense, the vortex weakens and eventually the zonal-mean wind reverses, initiating critical-layer interaction. There are different possible reasons behind the explosive growth of stratospheric wave activity that ultimately triggers/accompanies an SSW. The most often-invoked explanation is that anomalously intense planetary waves are forced in the troposphere and propagate into the stratosphere (Matsuno 1971; Polvani and Waugh 2004; Harnik 2009; Ayarzagüena et al. 2011; Nishii et al. 2009; Schneidereit et al. 2017; Díaz-Durán et al. 2017). A variety of different tropospheric phenomena have been shown to alter the stratospheric planetary wave patterns and contribute to the occurrence of SSW events—for example, tropospheric blocking (Martius et al. 2009; Woollings et al. 2010; Barriopedro and Calvo 2014), El Niño–Southern Oscillation (Barriopedro and Calvo 2014; Butler and Polvani 2011; Ineson and Scaife 2009), and the Madden–Julian oscillation (Liu et al. 2014). A different explanation for the rapid increase in wave fluxes during SSWs was proposed by Clark (1974), who suggested that SSWs may be the result of nonlinear resonant wave amplification within the stratosphere, favored by particular stratospheric flow configurations (see also Geisler 1974; Tung and Lindzen 1979; Plumb 1981; Smith 1989; Esler and Scott 2005; Matthewman and Esler 2011; Esler and Matthewman 2011). From this point of view, it is the vortex geometry that favors the development of an SSW event, and no anomalously intense tropospheric wave activity is needed to trigger the event. There is recent observational evidence that the vortex split of January 2009 may have been triggered by this mechanism (Albers and Birner 2014). Independently of the mechanism at work during a particular SSW, the potential influence of the stratosphere itself on the development of SSWs (sometimes referred to as vortex preconditioning) (McIntyre 1982; Smith 1992; Tripathi et al. 2015; Attard et al. 2016) is often obviated in the diagnosis of SSWs. Within the framework of the first mechanism, the lower stratosphere can act as a ''valve'' modulating the wave activity coming from the troposphere (Chen and Robinson 1992; Scott and Polvani 2004, 2006; Sjoberg and Birner 2014). Within the context of the second mechanism, the stratospheric flow configuration itself excites resonant growth of the internal/external normal modes.

This paper investigates the role of the stratospheric conditions prior to SSW events in a state-of-the-art climate model by addressing the following question: Does the tropospheric forcing that accompanies an SSW event in the model inevitably determine its occurrence? This question frames current efforts to deepen our understanding of the triggering mechanism of SSWs, with the broader goal of exploring the numerical models' skill in predicting such events and improving subseasonal and seasonal weather forecasts (Tripathi et al. 2015; Scaife et al. 2016). From the forecasting perspective, while some studies stress the key role of tropospheric wave activity for successful predictions of SSWs (Sun et al. 2012; Taguchi 2014), Taguchi (2016) has shown that skillful SSW forecasts depend on the ability of the model to predict the vortex geometry prior to the event, with split events being more challenging than displacement events. Using a multimodel ensemble approach to study the predictability of the SSW of January 2013, Tripathi et al. (2016) have found that while the models have a reasonably good skill in forecasting the tropospheric blocking that determined the tropospheric wave structure before the event, they still have limited skill in forecasting the SSW. In a predictability study of the SSW of January 2009, Noguchi et al. (2016) have suggested that the stratospheric conditions may be modulating to some extent the occurrence of this event.

The importance of stratospheric conditions in SSW development has been highlighted in several studies that employ simplified models to understand the fundamental dynamics of these events (Christiansen 1999; Scott and Polvani 2004, 2006). For example, Smith (1992) performed experiments with a primitive equation model of the stratosphere, changing the stratospheric conditions before two observed SSWs, but imposing the observed wave evolution in the lower boundary around 250 hPa. Her results emphasize that the lower-stratosphere winds are a better predictor of the SSWs analyzed than the tropospheric wave activity. Sjoberg and Birner (2014) used a modified version of the Holton–Mass model (Holton and Mass 1976) to investigate the positive wave–mean flow feedback, by which a wave activity convergence decelerates the zonal-mean wind, further allowing the upward propagation of wave activity. Their model configurations allowed a separation of the external and internal components of this feedback; the external feedback allows the model to draw wave activity upward from a limitless source below

the model bottom layer, while the internal feedback operates with the available wave activity within the model domain. Their results showed that model states with vacillation cycles (analogous to SSWs in this simplified model) exist even when the feedback is constrained to the model interior. Recently, Hitchcock and Haynes (2016) used a dry dynamical core model to investigate the stratospheric control on planetary waves during a large number of SSWs. One of their main conclusions is that the zonal-mean conditions in the stratosphere significantly control the wave growth that accompanies SSWs in their model but, also, that the troposphere needs to be in a favorable state for this wave amplification to occur.

In this paper, we test these ideas using the Whole Atmosphere Community Climate Model, version 4 (WACCM4). We follow a case study approach performing controlled experiments on modeled SSW events. The main methodological advantage of working with modeled SSWs, as opposed to observed SSWs, is the ability to decompose the dynamical evolution in an internally and physically consistent manner. Our experiments start three weeks before the occurrence of selected SSWs and are designed to maintain a fixed tropospheric evolution while allowing the stratosphere to evolve freely from different zonal-mean initial conditions. The uniqueness of these experiments lies on the isolation of the dynamical evolution of the stratosphere from the tropospheric wave injection, allowing us to separate the stratospheric control over the evolution of the wave field (and consequently the mean flow) in a comprehensive model. The six model cases analyzed indicate that the stratospheric conditions have the ability to substantially modify the development of SSWs in the model. However, the specific details of why this happens are different for each event, which in turn justifies the case study approach. Our results also call for caution with the widely used interpretation of the meridional heat flux at 100 hPa as indicator of the tropospheric wave injection into the stratosphere.

The remainder of the paper is organized as follows. Section 2 briefly introduces the model and describes the experimental setup. Section 3 presents results on six modeled SSW cases and examines two of them in more detail. The discussion and main conclusions are given in sections 4 and 5, respectively.

2. Model description and performance

a. WACCM

The Whole Atmosphere Community Climate Model (WACCM) is a state-of-the-art chemistry climate model developed at the National Center for Atmospheric Research (NCAR) and can be used as the atmospheric component of the Community Earth System Model (CESM). The version used in this study, WACCM4, has a 2.5° × 1.9° longitude–latitude grid, with the model top at about 140-km altitude. The vertical resolution ranges from 1.1 to 1.4 km in the troposphere and lower stratosphere to 3.5 km in the upper mesosphere and lower thermosphere. Garcia et al. (2007) and Marsh et al. (2013) provide a complete description of the model, and latest modifications to the chemistry module and to the orographic gravity wave drag scheme and their combined impact on the Antarctic cold-pole bias can be found in Solomon et al. (2015) and Garcia et al. (2017).

In this study, we use WACCM simulations performed for the Chemistry Climate Model Initiative (CCMI) exercise. In particular, we use four members of an ensemble with the REFC1 configuration, each of which is run over 60 yr (1955–2014) with prescribed sea surface temperatures from the Hadley Centre Sea Ice and Sea Surface Temperature dataset (HadISST; Rayner et al. 2003), and interactive chemistry. We will refer to these runs as base runs. For completeness, note that the base runs are the same set of WACCM simulations analyzed in Garcia et al. (2017) (where they are called REFC1-ORO), and they present a very good intraseasonal distribution of SSWs as compared to the reanalysis (Garcia et al. 2017).

b. Experimental setup

To explore the sensitivity of SSW events to the stratospheric-flow configuration, we perform model experiments with fixed tropospheric evolution (nudged winds and temperature in the troposphere) and varying stratospheric initial conditions. The experiments are performed with interactive chemistry to be consistent with the base runs, but there is no particular advantage in using a chemistry climate model for the purposes of this study. The procedure is as follows: We select different SSW events from the WACCM base runs; for each SSW selected, the model is restarted 21 days before the warming and run for 35 days, relaxing the winds and temperature below 10 km and the surface fluxes every time step to the corresponding base-run hourly fields; these will be our control runs (CTL). The choice of restarting the model 21 days before an SSW is motivated by the time scales of the wave forcing associated with the development of SSWs, which are typically longer than 10 days (Polvani and Waugh 2004; Sjoberg and Birner 2012). The nudging strength is given by a relaxation time of 50 h. We have checked that the nudging process does not introduce significant changes to the simulation of the SSW and found the SSW cycle in CTL and in the base run to be practically identical. Details on the nudging

procedure in WACCM can be found in Smith et al. (2017). It is important to remark that the nudging configuration in WACCM is built in such a way that the lid of the nudging region has to be a constant log-pressure altitude. Thus, our choice of locating the lid at 10 km ensures that the extratropical tropopause lies within this nudged region. Results obtained selecting a different top nudging altitude will be discussed in section 4.

For each SSW, a set of sensitivity experiments is then performed. The setup is similar to CTL, but this time we modify the initial stratospheric state, that is, 21 days before the SSW. We remark that the purpose is not to investigate the sensitivity to particular perturbations but to test the more qualitative assertion that the state of the stratosphere can influence the dynamical evolution into SSWs. A simple way to achieve this is by adding to the initial state a zonally symmetric zonal wind Δu and temperature ΔT in gradient wind balance:

$$\left.\begin{aligned}\Delta u &= \Delta u_m \exp\left[-\left(\frac{\phi-\phi_c}{\Delta\phi}\right)^2\right]\exp\left[-\left(\frac{z-z_c}{\Delta z}\right)^2\right]\\ -\frac{1}{a}\frac{\partial \Delta T}{\partial \phi} &= \frac{\partial}{\partial z}\left[\Delta u\left(f+\frac{2u_0+\Delta u}{a}\tan\phi\right)\right]\end{aligned}\right\}, \tag{1}$$

where a is Earth's radius, f is the Coriolis parameter, and u_0 is the initial, unmodified zonal-mean zonal wind.

The zonal-mean wind change specified by Eq. (1) is a Gaussian in latitude ϕ and log-pressure height z, with parameters $(\phi_c, \Delta\phi)$ and $(z_c, \Delta z)$, respectively, and maximum amplitude Δu_m. By altering the initial state with a balanced field, it is ensured that the model does not experience any fast adjustment at the beginning of the simulations (not shown). In addition, the longitudinal symmetry of Δu in Eq. (1) guarantees initial continuity of the wave field between the nudged and the free-evolving region.

Section 3 analyzes 18 experiments performed on six different SSW events: three displacements and three splits. Table 1 summarizes the combination of parameter values $(\Delta u_m, \phi_c, \Delta\phi, z_c, \Delta z)$ used in the experiments performed.[1] Basically, the location of the Gaussian center and the width and depth of Gaussian are varied for each experiment. Note that half the experiments have positive wind perturbations and half negative. The magnitude of Δu_m was chosen to be $\pm 10\,\mathrm{m\,s^{-1}}$ after finding that smaller values (e.g., $\Delta u_m = \pm 5\,\mathrm{m\,s^{-1}}$) did not disrupt the occurrence of the SSW in a sufficient number of experiments. The relatively large values of Δu_m required to disrupt SSWs follow from the strong constraints in our model setup, where the tropospheric fields are nudged to a particular evolution. We discuss further the magnitude of these changes to the initial fields and their success in altering the initial wave propagation conditions in section 4.

3. Case studies

a. A displacement event

The first case study is a February displacement event. Figure 1 shows the initial conditions in the zonal-mean zonal wind and temperature for the control experiment of this event (herein CTL-D1), together with one set of zonal wind and temperature perturbations (the one corresponding to the first column of Table 1; i.e., experiment 11).

Figure 2a shows the time–height section of the zonal-mean wind at 60°N, denoted U^{60N}, and the standardized anomalies of the vertical component of the EP flux F_z averaged over 45°–75°N for CTL-D1. The standardization of F_z aims at highlighting significant anomalies at different altitudes, and it is carried out by dividing at each point the daily anomalies by the daily climatological standard deviation σ. The zonal winds in the upper stratosphere have two deceleration periods: one at around two weeks before the warming, and the other a few days before the central date of the warming. The midstratospheric winds, on the other hand, follow a smoother evolution with a gradual deceleration starting 10 days before the central date. As happens in many displacement SSWs, the easterlies in this event appear at upper levels first and propagate downward in a matter of a few days (Charlton and Polvani 2007). The evolution of F_z presents strong positive anomalies during the whole 20-day period before the SSW, usually larger than 0.5σ. Particularly large are the values in the upper stratosphere and lower mesosphere (40–60-km height) around days −5 to −2, which occur simultaneously with the beginning of the wind deceleration at those altitudes.

Figure 2b compares the time series of U^{60N} at 10 hPa for the control run (CTL-D1, thick black line) with 18 experiments, all having different initial conditions in the stratosphere, as reported in Table 1. We have sorted the experiments in two groups according to whether an SSW occurs[2] (red lines) or fails to develop (blue lines). Notice

[1] Note that taking two different values for each of the five variables $(\Delta u_m, \phi_c, \Delta\phi, z_c, \Delta z)$ results in a total of 32 possible combinations. The 18 combinations used in this study have been selected arbitrarily.

[2] To determine the occurrence of an SSW, we simply check whether U^{60N} at 10 hPa crosses the zero-wind line for periods longer than 1 day.

TABLE 1. Values of the parameters of the Gaussian-shaped wind initial perturbation used in the model experiments. Experiments 11–19 have positive winds, and experiments 21–29 have negative winds.

	Expt																	
	11	21	12	22	13	23	14	24	15	25	16	26	17	27	18	28	19	29
Δu_m (m s^{-1})	10	−10	10	−10	10	−10	10	−10	10	−10	10	−10	10	−10	10	−10	10	−10
ϕ_c (°N)	60		60		45		45		60		60		45		60		45	
$\Delta\phi$ (°)	30		15		15		30		30		30		30		30		30	
z_c (km)	35		35		35		35		35		50		50		50		50	
Δz (km)	25		25		25		25		40		25		25		40		40	

that the latter group is composed of six experiments, all of them having an initial maximum perturbation amplitude of $\Delta u_m = -10\,\mathrm{m\,s^{-1}}$ (specifically, experiments 21–25 and 28 in Table 1). In the following, we will compute composites of different variables for the set of experiments that produce an SSW and the set that fails to produce one and analyze the differences. These composites will be referred to as SSW-CD1 and noSSW-CD1, respectively.

Figures 3a and 3b shows time–height evolutions of U^{60N} and F_z anomalies similar to Fig. 2a, but for the composites SSW-CD1 and noSSW-CD1. Also shown are F_z plots for single zonal wavenumber: $s = 1$ (Figs. 3c, d) and $s = 2$ (Figs. 3e,f). The composite evolution of U^{60N} as a function of height for SSW-CD1 is quite similar to CTL-D1 (Fig. 2a), unlike the evolution in the noSSW-CD1 composite. In the latter, the upper-stratospheric winds do not decelerate starting around day −15 (they actually accelerate) and follow a rather different evolution. This is also apparent in the F_z anomaly field; while in SSW-CD1 the strong positive F_z anomalies drive the wind deceleration at around day −15 (similarly to CTL-D1, Fig. 2a), in noSSW-CD1 the F_z anomalies are much attenuated. The persistent positive F_z anomalies during the 20-day period before the warming in SSW-CD1 are mainly due to the wave-1 component (Fig. 3c), though a couple of wave-2 events also contribute (Fig. 3e). The first of these wave-2 events has a peak value over 2.75σ and is a main contributor of the wind deceleration starting at day −15. The second wave-2 event has a peak value of 0.75σ localized in the mid- to upper stratosphere (30–50 km) during the development of the SSW. It is clear from Figs. 2 and 3 that the paths followed by the SSW-CD1 and noSSW-CD1 composites diverge from each other early in the simulations. A plausible hypothesis is then that the changes in wind configuration in the lower stratosphere at the beginning of the runs give rise to significant changes in wave–mean flow interactions. In fact, the composite wind in the lower stratosphere has a very different vertical shear in SSW-CD1 and noSSW-CD1, and the vertical penetration of the wave-1 component is much deeper in the former than in the latter composites during the first 10 days of the experiments (Figs. 3c and 3d).

To further explore this hypothesis, Fig. 4 shows composite EP flux diagrams at different days (from day −20 to −10). First, while the zonal-mean winds above 30 km are relatively similar in days −20 and −18

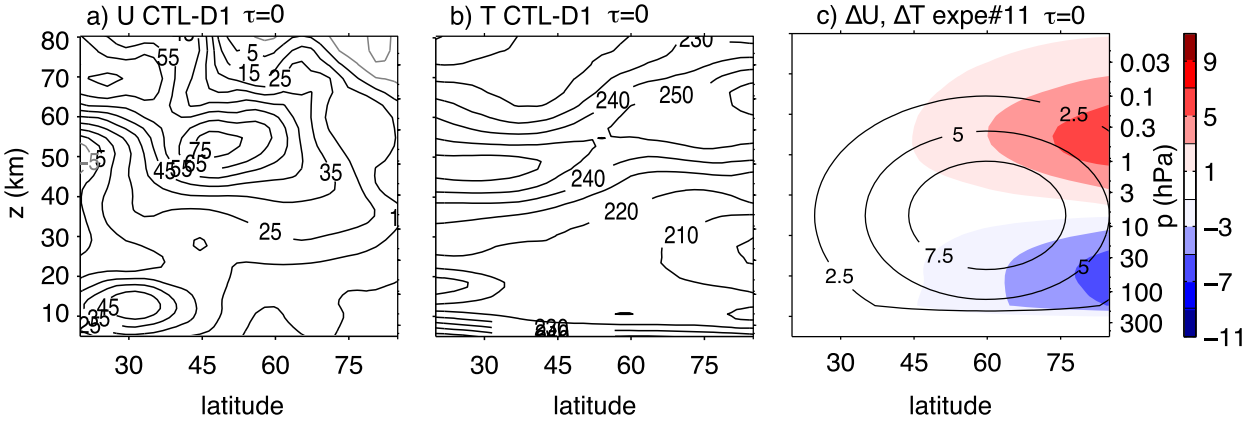

FIG. 1. Initial zonal-mean profiles of (a) zonal wind (m s^{-1}) and (b) temperature (K) in the displacement event analyzed in section 3a (CTL-D1). (c) Zonal-mean perturbations to the initial conditions of zonal wind (contours; m s^{-1}) and temperature (shading; K) for experiment 11. See text and Table 1 for details.

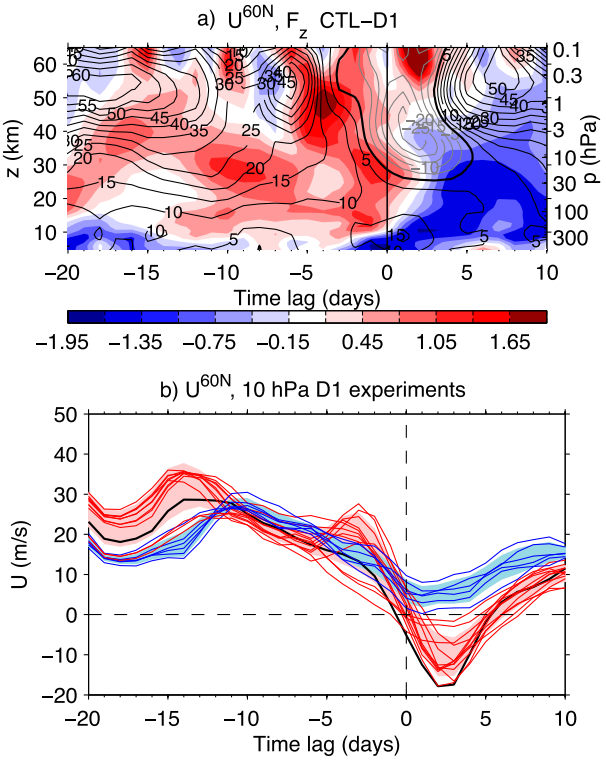

FIG. 2. (a) Time–height evolution of the zonal-mean wind (contours) at 60°N, and the standardized anomalies of the EP flux vertical component (shading) averaged over 45°–75°N, for CTL-D1. Contour interval is 5 m s^{-1}, with the zero-wind line in bold; F_z units are multiples of 1σ, with a 0.3σ interval starting at $\pm 0.15\sigma$. (b) Zonal-mean zonal wind (m s^{-1}) at 60°N and 10 hPa as a function of time lag about the SSW central date in CTL-D1 (thick black line). Light red (blue) shading represents $\pm 1\sigma$ around the mean of experiments with (without) an SSW.

in the two sets of experiments, in the polar lower stratosphere the winds have a stronger westerly component in SSW-CD1 than in noSSW-CD1, consistent with the imposed anomalies. Indeed, an easterly anomaly grows during these days in the lower polar stratosphere in both composites, but while it fades away and the westerlies resume in SSW-CD1 (Fig. 4a), the easterly anomaly lasts until day −12 in noSSW-CD1. This different flow configuration in the lower stratosphere has a strong impact on the wave driving. For SSW-CD1 (Fig. 4a), a strong negative EP flux divergence at 40–50 km from day −16 to day −12 is associated with a deceleration of the upper-level winds, and it aligns the jet more vertically over the pole. By day −10 the westerly jet maximum has moved downward and poleward (40-km height and 75°N), a configuration identified in previous studies as preconditioned to subsequent SSW triggering (e.g., Smith 1992). For noSSW-CD1 (Fig. 4b), the upward-propagating waves are deflected toward lower latitudes by the easterly winds in the lower stratosphere, and the strong wave driving present in SSW-CD1 in the polar latitudes at day −14 and on does not appear here. As a result, the upper-level winds in noSSW-CD1 do not decelerate, and the jet is in a completely different vertical and latitudinal configuration by day −10.

Figure 5 shows the times series of F_z at 300, 100, and 10 hPa for CTL-D1 and each of the experiments. We note that these are not anomalies with respect to the climatology; they are the actual F_z time series. The 300-hPa level is located in the upper troposphere below 10 km—thus, in the nudging region. Consequently, all time series at 300 hPa present virtually identical evolutions. Clear differences arise already at 100 hPa despite the very similar F_z below, including the sudden growth of F_z in CTL-D1 and the experiments with warming at day −2 to values up to 2 times as large as in the experiments without warming. This can be regarded as an example of the internal feedback discussed by Sjoberg and Birner (2014) in the context of the Holton–Mass model, whereby a favorable mean state enhances the upward flux of wave activity available within the model domain.[3] That is, the different stratospheric zonal-mean states in SSW-CD1 and noSSW-CD1 condition F_z at 100 hPa. At 10 hPa, differences between the two sets of experiments are sharper from day −15. These results emphasize the necessary role of the stratospheric basic flow on the differing evolutions of the wave fields in the experiments analyzed.

b. A split event

The next case is a January split event. Figure 6a displays the time–height evolution of U^{60N} and the standardized anomalies of F_z averaged over 45°–75°N for the split-event control case, CTL-S1. The profile shows a strong deceleration of stratospheric winds for about a week starting 17 days before the sudden warming, which ends with the development of rather intense upper-stratospheric easterlies (peak of −25 m s^{-1}, day −9) and a zero-wind line located at about 40-km height from 10 to 5 days before the warming. After this event, the upper-stratospheric westerly winds slowly recover, and the 10-hPa winds start decelerating at day −4 during the onset of the SSW event. There are two distinct periods of upward-propagating wave fluxes in the stratosphere during this 20-day interval preceding the SSW. The first one extends throughout the whole depth of the

[3] In the context of our model experiments, we interpret this feedback as an "internal" process in the stratosphere since the wave activity flux F_z in the troposphere is the same in all the experiments for a given SSW case.

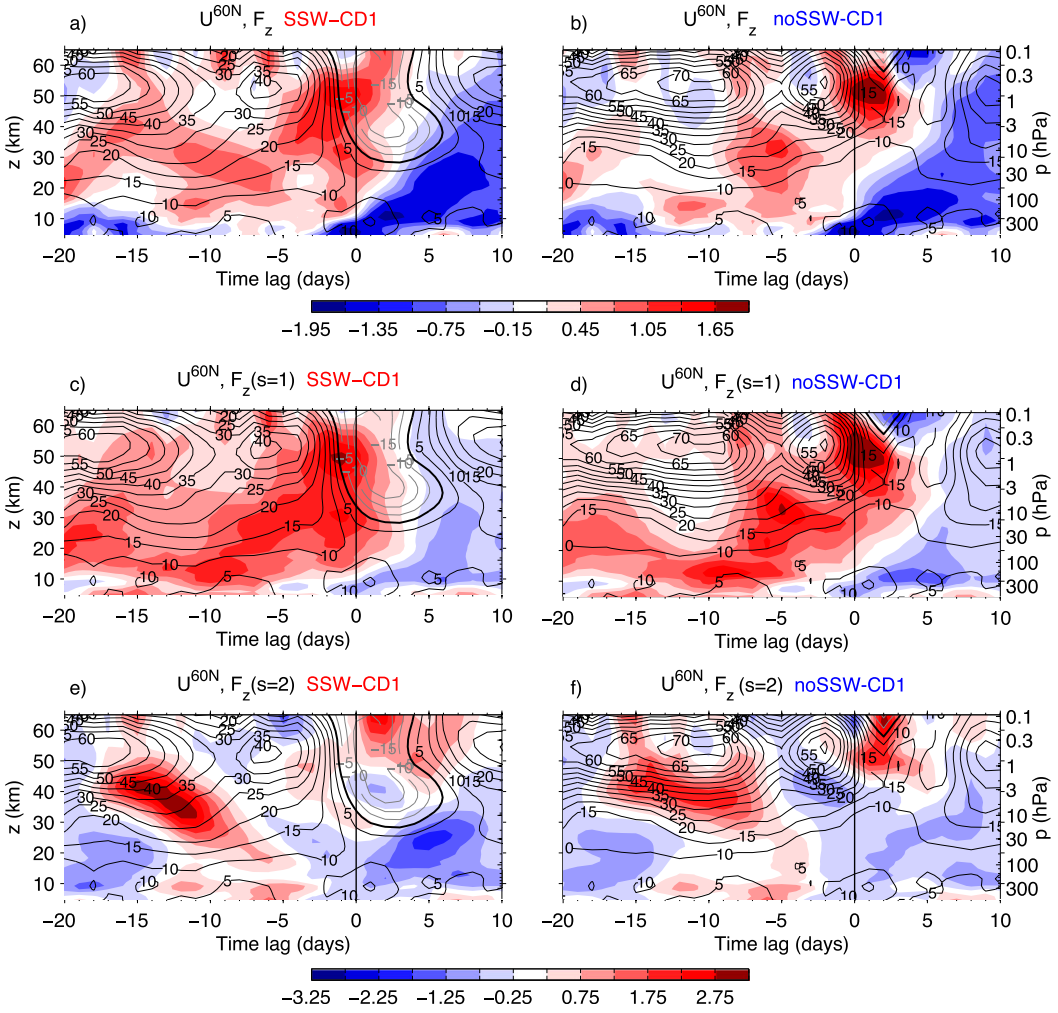

FIG. 3. As in Fig. 2a, but for the composites (a),(c),(e) SSW-CD1 and (b),(d),(f) noSSW-CD1. (top) Total F_z anomaly, (middle) wave-1 ($s = 1$) component, and (bottom) wave-2 ($s = 2$) component of F_z anomaly.

stratosphere and coincides with the development of the upper-level easterlies, likely producing the associated deceleration. The second one is much shallower and is related to the SSW itself. The positive F_z anomalies appear first in the upper troposphere/lower stratosphere at day −7 and then propagate upward.

Figure 6b compares the time series of U^{60N} at 10 hPa for CTL-S1 (thick black line) with 18 experiments (see Table 1). In this set of experiments, 10 recover the SSW with the central date delayed about 1 day (red lines) and 8 of them do not simulate the SSW (blue lines; these latter are experiments 11 and 13–19 in Table 1). In this SSW case, the sign of the initial wind alterations in the experiments with no warming is positive, opposite to that in the displacement case study analyzed in the previous section (Fig. 2b). Aside from the different wind magnitude of the two sets of experiments, U^{60N} presents a similar timing and magnitude of acceleration and deceleration in all the experiments until day −5.

The horizontal dynamical evolution of the vortex during the experiments can be analyzed with potential vorticity maps. Figure 7 shows the vortex edge at 850 K (around 30-km altitude), identified as the 36 potential vorticity unit (PVU; 1 PVU = 10^{-6} K kg^{-1} m^2 s^{-1}) isoline of the generalized potential vorticity (PV) (Müller and Günther 2003) for different days of the simulations. Despite the differences in zonal-mean winds (Fig. 6b), the vortices in CTL-S1 and all experiments display very similar shapes until day −10. Larger differences show up from day −6 onward, when CTL-S1 transitions to an elongated, "pinched" vortex (day −4), and finally a split (day 0). While the vortices in the experiments with SSW are located in the Western Hemisphere over northern North America and experience a massive loss of vortex area from days −6 to 0, the vortices without SSW keep

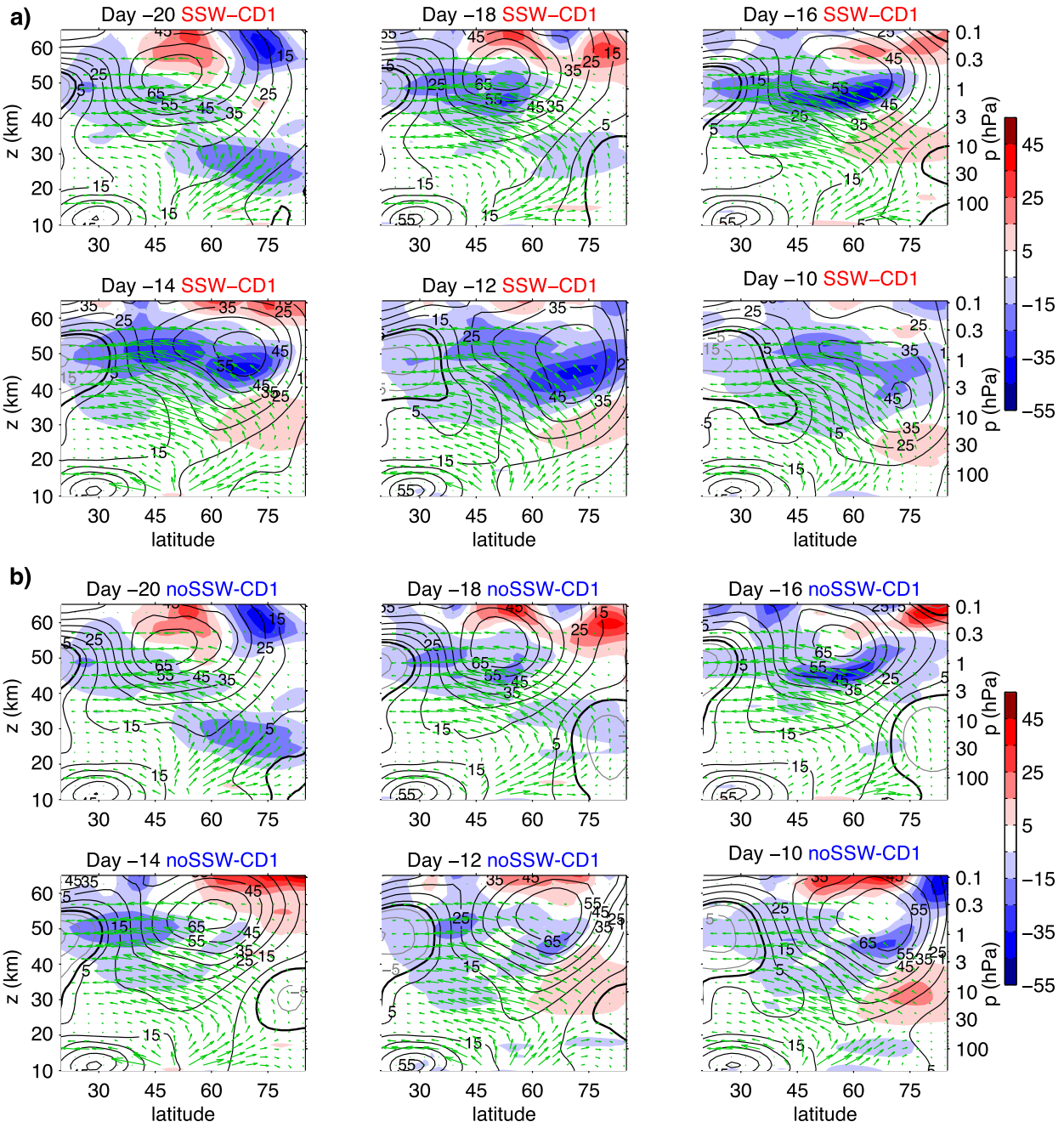

FIG. 4. Composites of EP flux diagrams (latitude–height) for (a) SSW-CD1 and (b) noSSW-CD1, at different time lags as indicated. Arrows are EP flux vectors. Contours are zonal-mean zonal wind (contour interval is 10 m s^{-1}, starting at ±5 m s^{-1}), and the thick black line is the zero-wind line. Shading shows EP flux divergence weighted by the inverse of $\rho_o a\cos\phi$ [i.e., wave forcing, with $\rho_o = \rho_o(z)$ the background density; m s^{-1} day^{-1}].

their northern Eurasia location and maintain a more coherent structure until day 0. Although there are differences in the strength of the winds at 60°N and 10 hPa among the two sets of experiments (i.e., with and without an SSW) due to the initial conditions, the differences in vortex shape and location are quite subtle right until the deceleration of the midstratospheric winds starts at around day −6 (Fig. 6b).

As in the previous case study, we next perform a composite analysis, and the composites for the experiments with and without the warming will be referred to as SSW-CS1 and noSSW-CS1, respectively. Figure 8

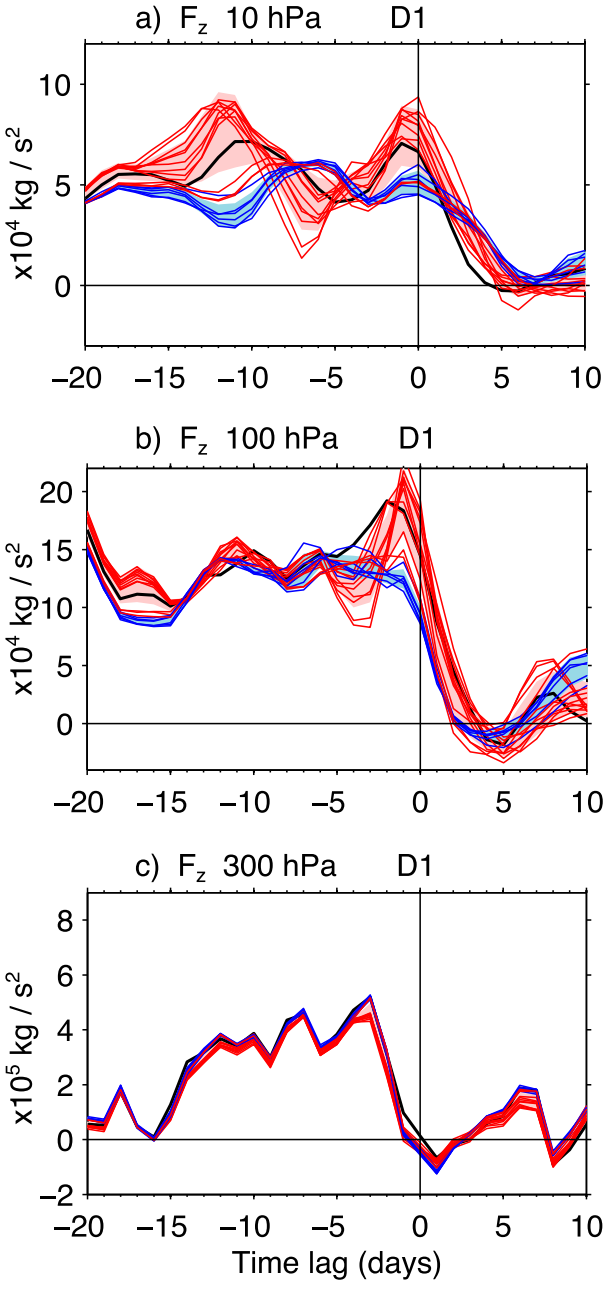

FIG. 5. Time series of the vertical component of the EP flux (kg s^{-2}), averaged over 45°–75°N, for the experiments on the D1 case, at (a) 10, (b) 100, and (c) 300 hPa. Experiments with and without the sudden warming are colored in red and blue, respectively, and the control run is in black.

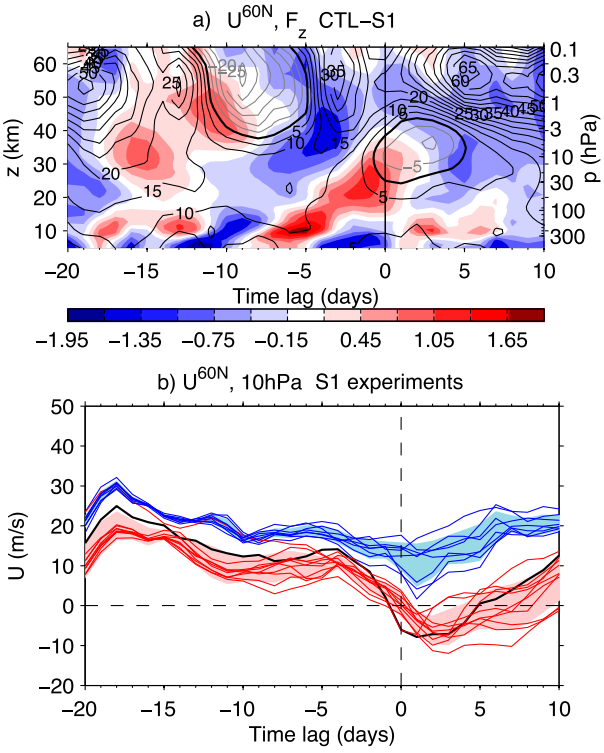

FIG. 6. As in Fig. 2, but for CTL-S1.

(top) displays the time–height evolution of the winds at 60°N and F_z anomalies composited for the two sets of experiments. The winds are a bit stronger in noSSW-CS1 throughout the column during the first few days, consistent with the imposed changes to the initial conditions. In spite of this, from days −20 to −10 the evolutions of U^{60N} and F_z are very similar in the two composites, as well as similar to CTL-S1 (Fig. 6a). However, there are remarkable differences starting at around day −7. We do see the upward wave event that starts in the lower stratosphere at day −7 in both composites. However, while in SSW-CS1 it follows a similar evolution to CTL-S1, albeit weaker in magnitude (see Fig. 6b), in noSSW-CS1 its vertical penetration decays at around day −4 and there is no burst of stratospheric wave activity anomalies from that day on. The middle and bottom panels of Fig. 8 show similar plots but for the zonal wavenumbers $s = 1$ and $s = 2$, respectively. The first wave event has a strong $s = 1$ component, while the wave event that triggers/accompanies the sudden warming is clearly dominated by the $s = 2$ component, consistent with a splitting vortex. And again, the magnitude and vertical extension of this last wave-2 event is larger in SSW-CS1 than in noSSW-CS1.

Figure 9 displays the time series of F_z at different altitudes for CTL-S1 and the corresponding experiments. Consistent with the experimental setup, the evolution of F_z at 300 hPa is similar in SSW-CS1 and noSSW-CS1, albeit small differences are evident. The 100-hPa fluxes are modified throughout the evolution of the runs, and a large difference appears right before day 0; in CTL-S1 and experiments with SSW (red lines) the wave event peaking at day −4 extends in time past day 0, but in the experiments without SSW (blue lines) the event decays

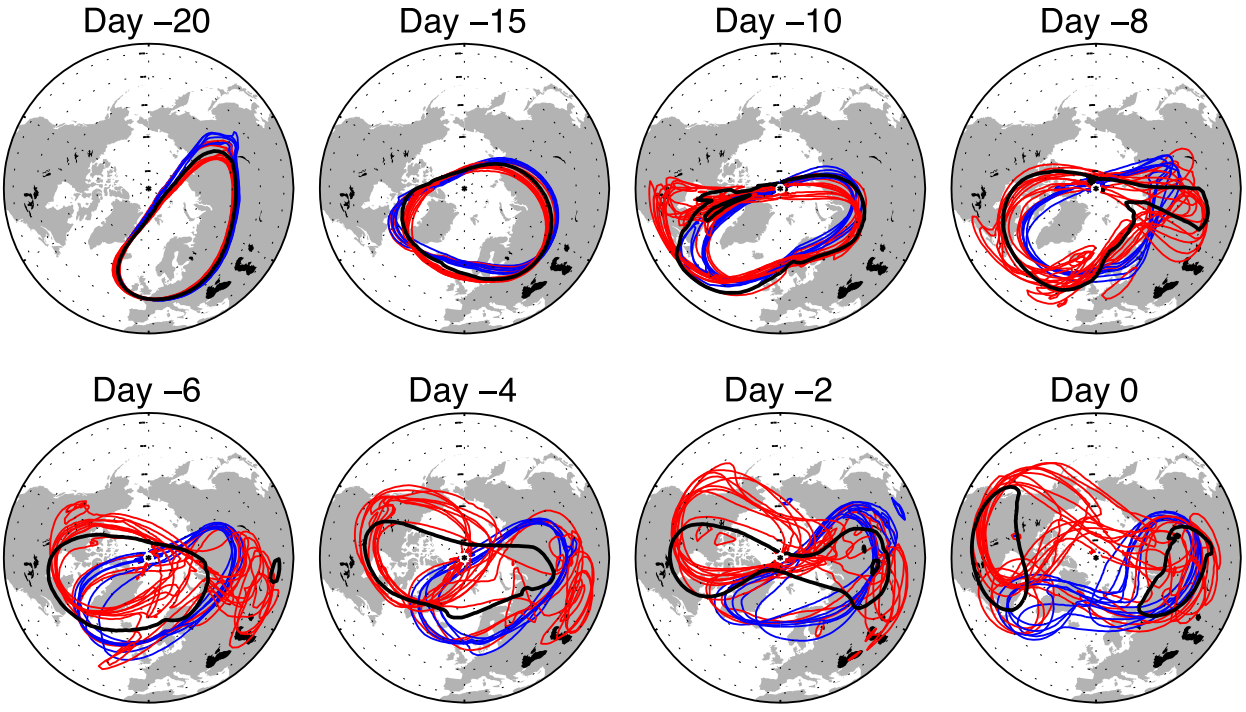

FIG. 7. Vortex edge defined by the isoline of the 36-PVU Lait's PV at 850 K for CTL-S1 (black), experiments with SSW (red), and experiments with no SSW (blue) for different days before the central day of the warming in CTL-S1.

right after the peak. Since all the experiments have a very similar upper-tropospheric wave flux (Fig. 9c), we can infer that the above stratospheric differences are of stratospheric origin. The ultimate causes of the disparities are perhaps not as clear as in the displacement case analyzed in the previous subsection. Figure 10 shows EP flux diagrams ($s = 2$ component) at different days from day -10 to day -1 for the two sets of experiments. There are two noticeable features in these plots. The first is the longer persistence of the upper-stratosphere easterly event in SSW-CS1, as noted in the discussion of Fig. 8. By the end of this event at day -4, the noSSW-CS1 composite presents a stronger jet structure at 60°–75°N, particularly in the lower stratosphere, which can channel the waves upward and away from high latitudes. Indeed, the wave forcing (negative EP flux divergence) in the midstratosphere (60°–75°N, 30–3 hPa) is stronger at days -2 and -1 for the SSW-CS1 composite, triggering the sudden warming.

The second noticeable feature is the lack of clear evidence explaining why the EP fluxes are larger in SSW-CS1 than in noSSW-CS1 at day -2 and -1 between 20 and 40 km, given that all the experiments have a similar tropospheric forcing (Fig. 9c). It is possible that the larger fluxes in SSW-CS1 arise from local instabilities in the lower stratosphere, but the narrow band of EP flux divergence above 10 km shows very similar values in both composites. It is also possible that the highly distorted vortex during these days reaches a geometry that favors resonant wave growth, as suggested by Matthewman and Esler (2011) (we do see a "peanut shaped" vortex for CTL-S1 at day -2 in Fig. 7, but this is not as clear in the experiments with a warming). Although rigorous proofs of these possibilities are difficult and beyond the scope of the paper, the essential role of the stratosphere is clear in these tests, which in turn confirms the hypothesis that the stratosphere is not just passively responding to a given tropospheric forcing during the development of an SSW.

c. *Experiments on other SSW cases*

In the previous subsections, we analyzed in some detail the dynamics of model experiments for two SSW cases and concluded that the occurrence of these two SSWs is not uniquely determined by the tropospheric evolution. This subsection describes additional experiments that suggest this conclusion may be extrapolated to other SSW events in our model. Figure 11 shows the U^{60N} evolution at 10 hPa of four other SSW cases, two vortex displacements (D2 and D3) and two splits (S2 and S3), and the corresponding evolutions for the model experiments with wind and temperature changes to the initial state given in Table 1. There are two commonalities with the events previously analyzed. First, there are

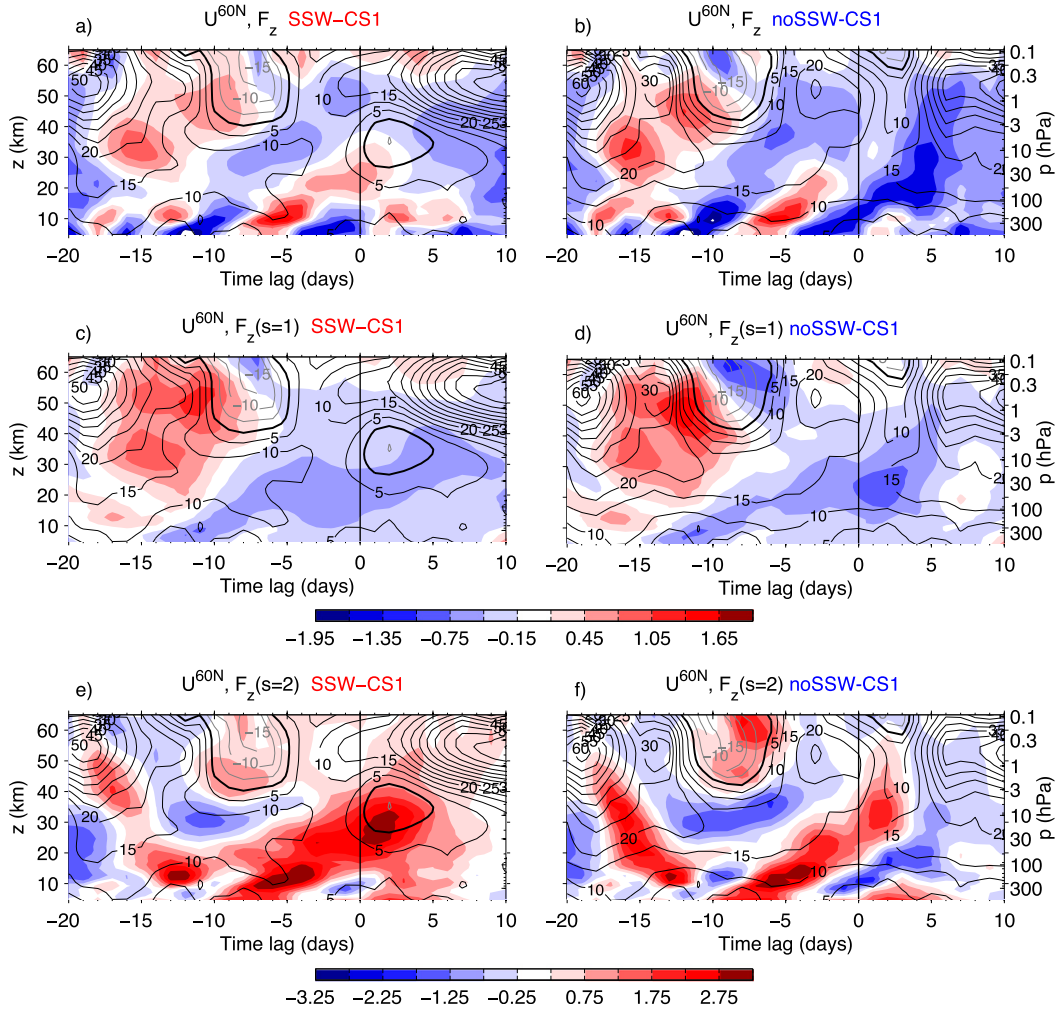

FIG. 8. As in Fig. 3, but for the S1 case study.

experiments that do not develop an SSW, although the number varies among cases. And second, for each control SSW explored, the experiments that prevented the SSW from occurring have the same sign of the wind changes to the initial conditions; but across different control SSWs the sign of those initial wind changes is not the same. That is, it cannot generally be said that all negative initial wind changes prevent the SSW; but for each individual SSW there is a definitely signed wind perturbation that can prevent it (negative for the three displacements and one split and positive for two splits).

The left column in Fig. 12 displays the vertical evolution of U^{60N} and the standardized anomalies of F_z in the CTL run for each case. These plots illustrate the different wind and wave-field evolutions that lead to an SSW in each case. For example, CTL-D2 (Fig. 12a) presents a wind evolution somewhat similar to CTL-D1 (Fig. 2a) with intense winds in the stratopause region (~50 km) that strongly decelerate at around day −5 and negative winds showing up at upper levels first and in the midstratosphere a few days later. On the other hand, CTL-S2 presents a very different wind evolution with a very shallow region of negative winds around the central warming date. As expected, all warming events have in common an enhanced positive anomaly of F_z starting a few days before day 0 that typically exceeds 0.75σ (Figs. 12a,c,e,g), although the vertical depth, duration, and intensity of these wave events are case dependent. The right column in Fig. 12 shows the corresponding noSSW composites and reveals the variety of reasons why the warming does not develop in these experiments. For example, noSSW-CD2 reproduces a strong wave event that starts at around day −3 that is consistent with the wind deceleration throughout the stratosphere (Fig. 12b), but neither the wave event nor the wind deceleration are as intense as in CTL-D2 (Fig. 12a), and

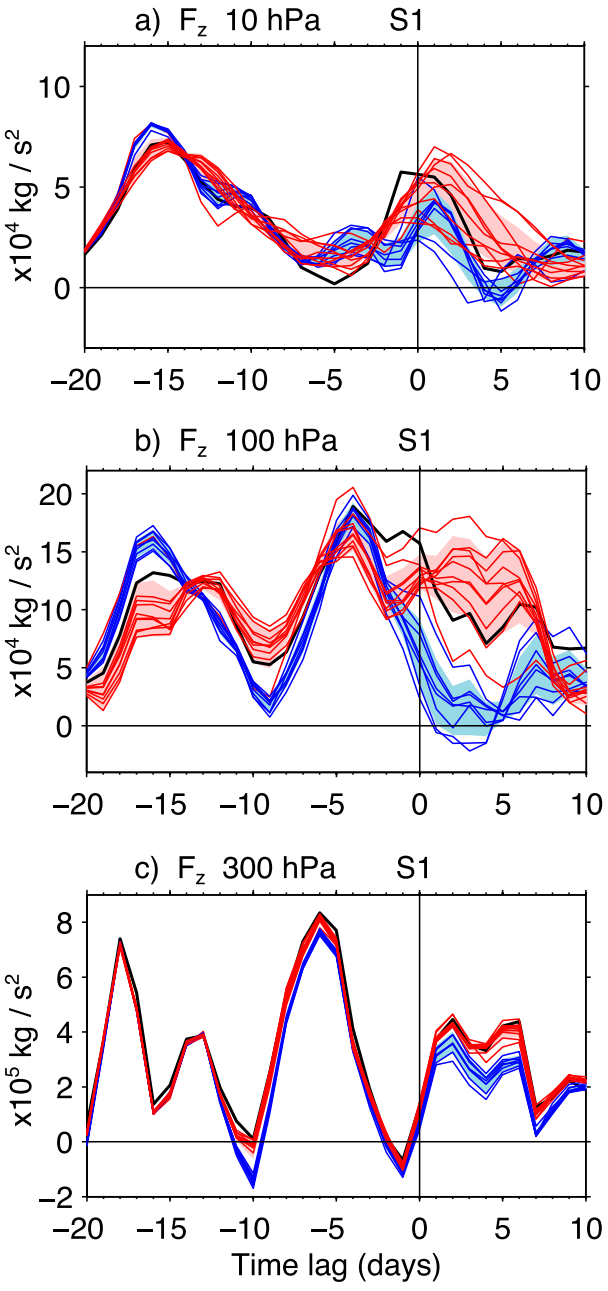

FIG. 9. As in Fig. 5, but for the S1 case study.

the negative winds do not appear. A radically different behavior appears in noSSW-CS2 (Fig. 12f), where the anomalous wave event that accompanies the SSW in CTL-S2 is not reproduced at all and the stratospheric flow does not experience any deceleration.

The systematically weaker, or in the S2 case the absence of, positive F_z anomaly around lag 0 in the noSSW composites of Figs. 3, 8, and 12 is a clear indication that tropospheric wave injection is not the only factor determining the stratospheric wave growth immediately preceding an SSW (since the tropospheric wave flux is nearly identical in all experiments for a given SSW case). Processes such as the feedback between the mean flow and the available wave activity flux internal to the stratosphere, as described by Sjoberg and Birner (2014), may be relevant to understand the wave growth during SSWs in our model. In fact, the partial suppression of this feedback in the experiments with no SSW, caused by differences in the stratospheric mean flow, could explain the above-mentioned weaker positive F_z anomalies in the stratosphere around lag 0 in those experiments (Fig. 12).

4. Discussion

The results of section 3 can be summarized by noting that they highlight the important role of the stratosphere in the development of the modeled SSWs studied. Alternatively, one could argue that, despite relatively large alterations to the stratospheric initial conditions, the tropospheric forcing determines in great part the development of these SSWs because over half of the experiments analyzed in section 3 reproduce the SSW. Although both conclusions appear valid, there are certain characteristics of the experimental setup that encourage us to interpret the results as first stated, that is, emphasizing the importance of the stratospheric state. From a technical point of view, we are able to do a perfect bit-by-bit restart with WACCM, meaning that exactly the same atmospheric evolution as the control run is reproduced (and thus the development of the SSW is guaranteed) unless something is changed in the experiments. There are also a couple of important aspects from a more physical point of view. First, we heavily constrain the system by imposing the tropospheric evolution (below 10 km) that accompanies the SSWs studied, which is known to influence the stratospheric circulation variability, so if the occurrence of SSWs were solely controlled by the tropospheric wave forcing we would expect SSWs in all members. Second, the magnitude of the wind changes imposed on the initial conditions might seem large [$\Delta u_m = \pm 10\,\mathrm{m\,s^{-1}}$ in Eq. (1)], but these alterations may be changing weakly the (linear) wave propagation conditions. In fact, we noted in section 2 that using $\Delta u_m = \pm 5\,\mathrm{m\,s^{-1}}$ was not effective in preventing the warming from happening in most instances, which suggests that wind changes of this magnitude and shape do not alter wave propagation significantly. This can be illustrated by diagnosing the $s = 0$ (quasigeostrophic) index of refraction squared Q_0 (Matsuno 1970). Figure 13 displays composites of Q_0 on the first day of the runs for experiments with $\Delta u_m = \pm 10$ and $\pm 5\,\mathrm{m\,s^{-1}}$ and for CTL-S1. Note that the 18

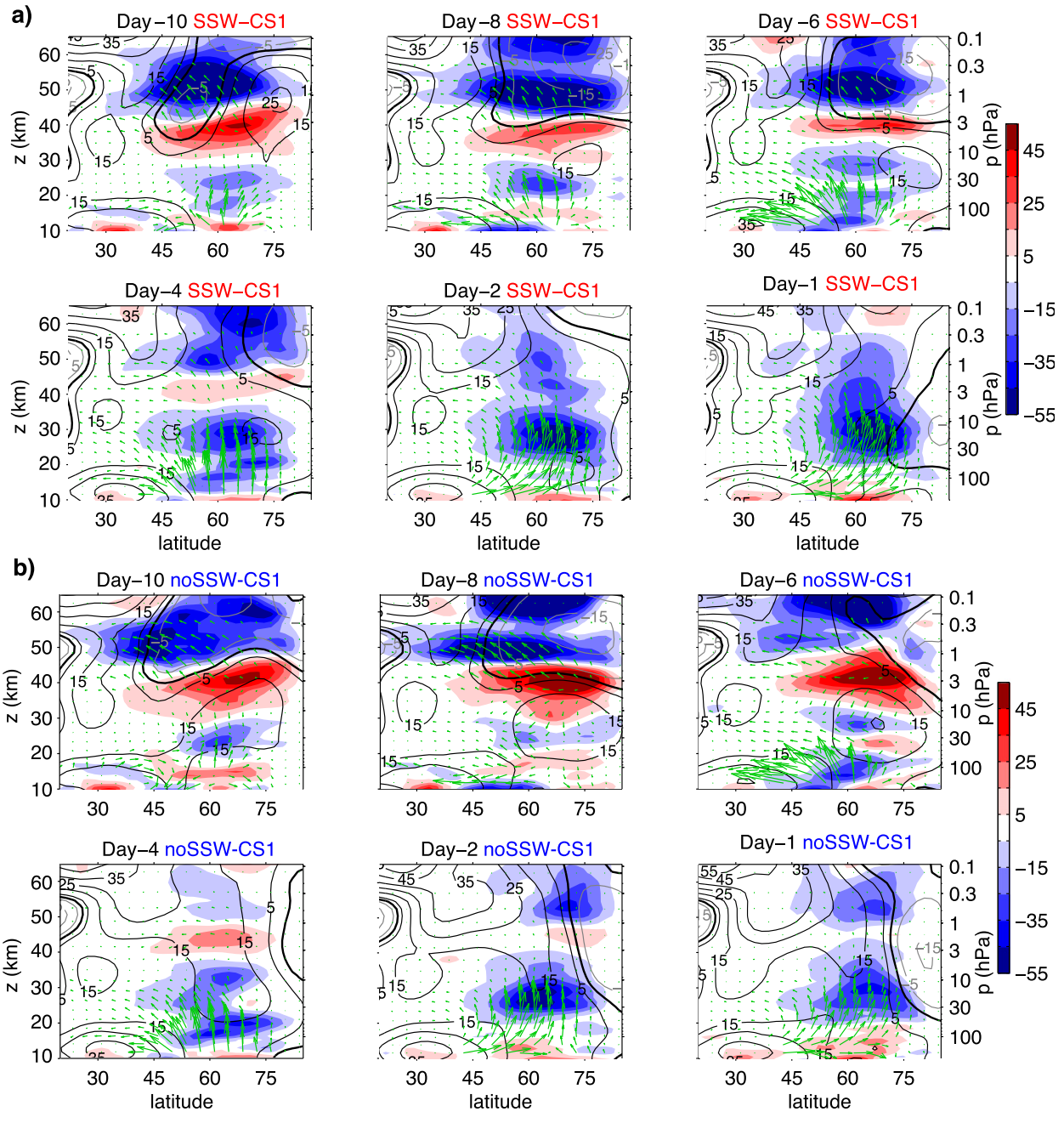

FIG. 10. As in Fig. 4, but for the $s = 2$ component of the EP flux for SSW-CS1 and noSSW-CS1 composites.

experiments performed with $\Delta u_m = \pm 5\,\mathrm{m\,s^{-1}}$ are similar to those reported in Table 1 (except for the value of Δu_m), and all of them produce SSWs in the S1 case. The structure of Q_0 is practically unchanged across all these plots, and only subtle differences in magnitude are present. This points out that, despite relatively large wind and temperature changes in the initial conditions, the differences in wave flux F_z between SSW-CS1 and noSSW-CS1 composites analyzed in section 3 (Fig. 8) arise from small differences in the initial linear wave propagation conditions (Fig. 13). Further, this may also be an indication that the onset of SSWs is highly nonlinear, and linear diagnostics such as the index of refraction should be interpreted with caution.

All these aspects favor the occurrence of the warming events in our experiments, so the fact that the events fail to occur in a substantial number of experiments (only if $\Delta u_m = 10\,\mathrm{m\,s^{-1}}$) implies that changing the stratospheric

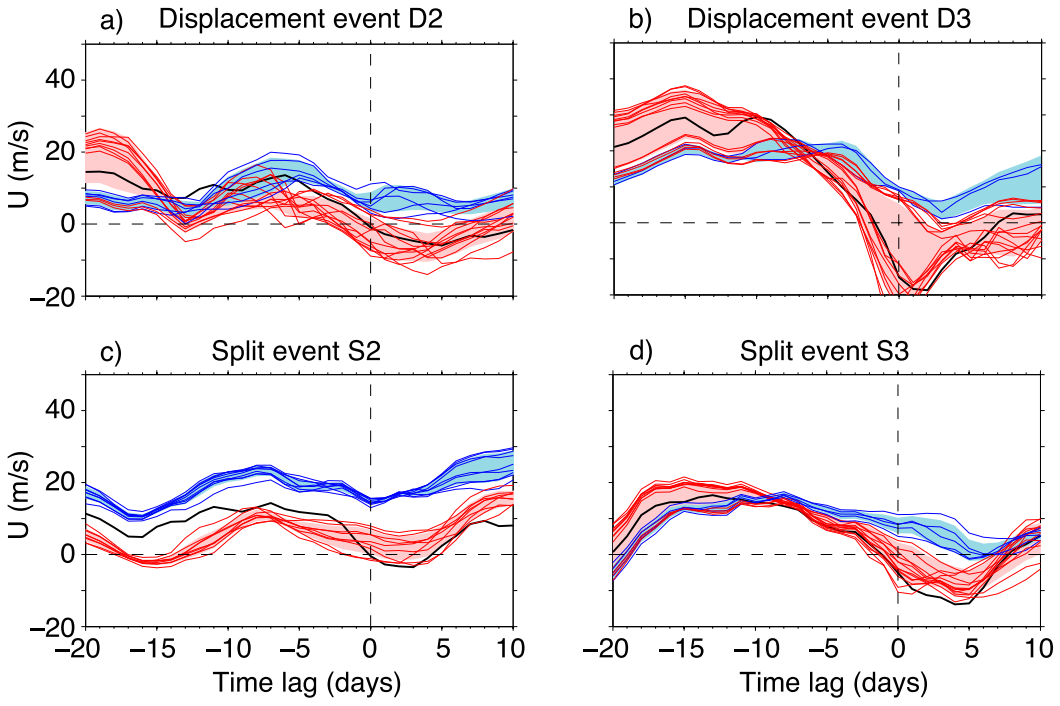

FIG. 11. As in Figs. 2b and 6b, but for four other SSW events in WACCM.

state can truly alter the development of an SSW. Nevertheless, we do not intend to dismiss the significance of the tropospheric wave injection but, rather, point out that a given tropospheric forcing without the "right" stratospheric state may not trigger an SSW, as suggested by several previous studies (McIntyre 1982; Smith 1992; Hitchcock and Haynes 2016). In this sense, the results by Martius et al. (2009) are illustrative: while most of the SSWs observed in the period 1957–2001 were preceded by the occurrence of tropospheric blocking anticyclone events, the opposite is not true: only 7% of blocking events were associated with an SSW. Also, Tripathi et al. (2016) noted that the models that forecast the SSW more accurately had smaller lower-stratospheric initial wind biases.

The search for tropospheric precursors to SSWs is motivated to a large extent by the need to improve the prediction skill of the models in seasonal and subseasonal forecasts. A common practice is to interpret the meridional heat flux (or, more generally, the vertical component of the EP flux F_z) at 100 hPa as indicative of incident wave activity from the troposphere into the stratosphere. Here, we question this interpretation; 100 hPa at extratropical latitudes lies well within the stratosphere, and the heat flux there is inevitably influenced by the stratospheric circulation and not only by wave propagation from below, as clearly demonstrated in Figs. 5 and 9, where differences in F_z at 100 hPa are identified between experiments with and without the SSW despite the troposphere being strongly constrained. But how critical are those differences in the heat flux at 100 hPa for the events analyzed? To answer this question, we have performed a few more experiments using the initial conditions of the runs that did not produce a sudden warming in each of the six events studied (blue lines in Figs. 2b, 6b, and 11), but now raising the nudging region up to 18 km (just above 100 hPa). The results for D1 and S1 cases are shown in Fig. 14. The zonal-mean winds at 60°N and 10 hPa in the experiments now present a very similar evolution to the control runs for both events, and all experiments develop an SSW (Figs. 14a,b). The behavior of F_z at 100 hPa is constrained by the nudging procedure (Figs. 14e,f), and F_z at 10 hPa follows quite closely the evolution in the control runs (Figs. 14c,d). Similar results are obtained with CTL-D3 and CTL-S3, while two experiments with CTL-D2 and nine with CTL-S2 with nudging up to 18 km still do not develop the warming (not shown). This indicates that the chances of reproducing the SSW are increased in our model if the nudging region extends to 18 km, but even this does not determine entirely the occurrence of the warming in the events studied.

We further explore the statistical connection between the upper-tropospheric and the stratospheric wave activity in WACCM by computing the squared coherence

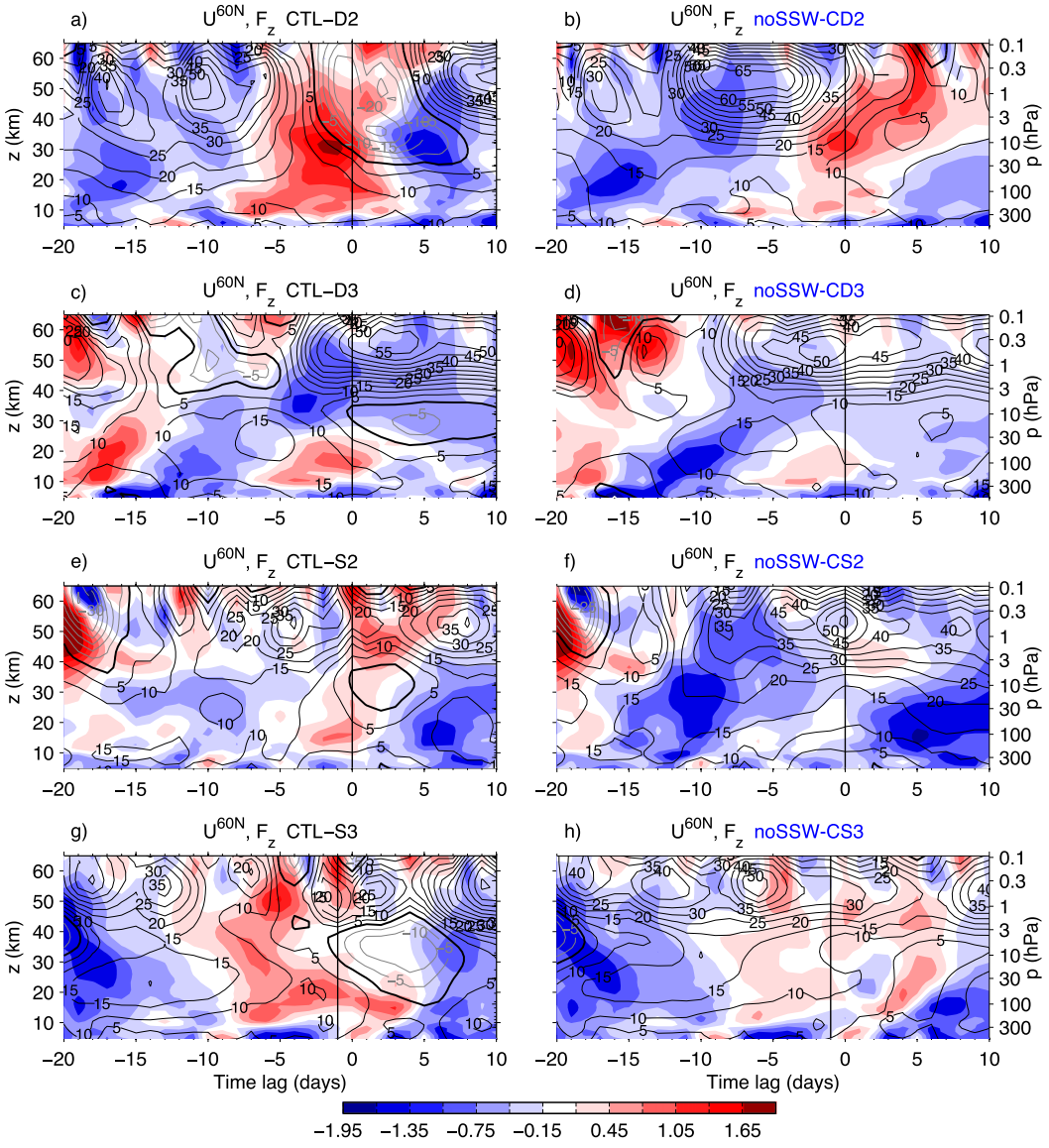

FIG. 12. Time–height evolution of the zonal-mean wind (contours; interval is 10 m s^{-1}) at 60°N, and the standardized anomalies of the EP flux vertical component (shading; multiples of 1σ) averaged over 45°–75°N for (a) CTL-D2, (c) CTL-D3, (e) CTL-S2, and (g) CTL-S3 and for (b) noSSW-CD2, (d) noSSW-CD3, (f) noSSW-CS2, and (h) noSSW-CS3.

of the October–March times series of F_z (for zonal wavenumbers 1 and 2) averaged over 45°–75°N at 300 and 100 hPa with the corresponding time series at different altitudes (Fig. 15). The squared coherence expresses the amplitude of the cross spectrum of two time series in dimensionless units (von Storch and Zwiers 1999). Being formally similar to a (squared) correlation coefficient, it can help us elucidate the frequencies at which the time series of F_z at 300 and 100 hPa maximize the covariance with F_z at other pressure levels. The coherence has been computed separately for winters with and without SSWs in all four WACCM base runs (240 simulated years in total), but the differences between these two sets of winters are small (cf. Fig. 15a with Fig. 15b and Fig. 15c with Fig. 15d). The squared coherence of F_z at 300 hPa with F_z at all other altitudes (Figs. 15a,b) has a value of 1 at 300 hPa, as expected, with decreasing values above and below. In the stratosphere, we see that 1) the squared coherence is higher for lower frequencies, particularly for periods longer than 20 days, and 2) it decreases very rapidly in the lower stratosphere, with values of around 0.2–0.4 at 100 hPa

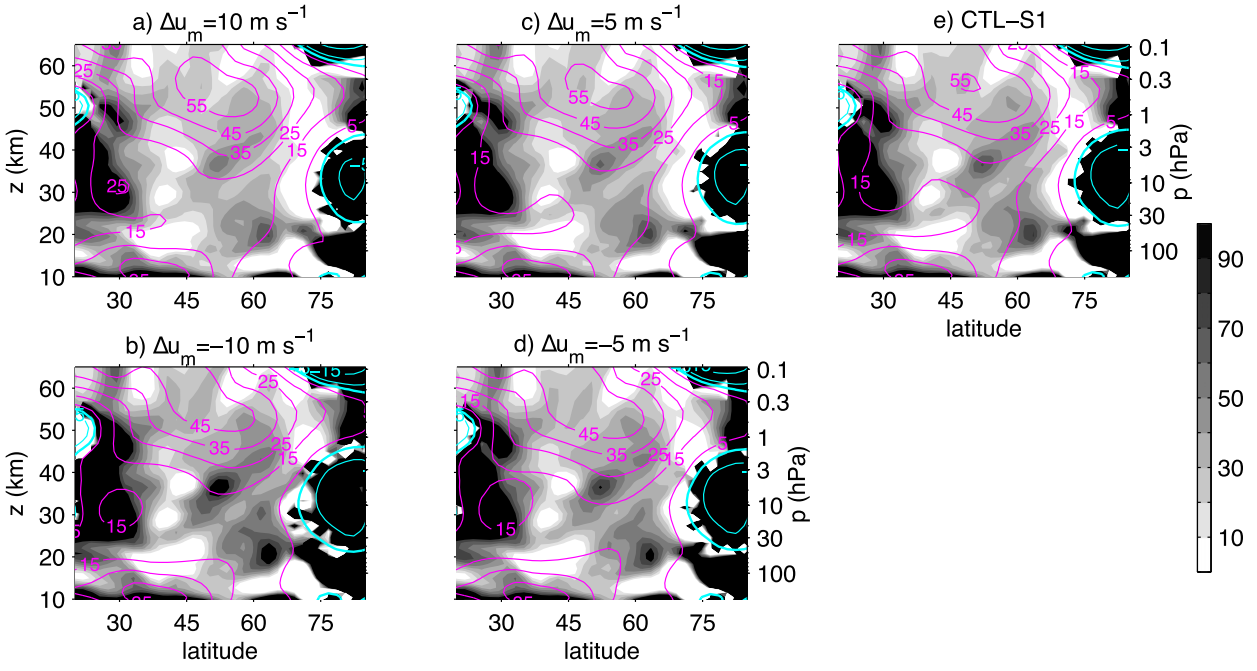

FIG. 13. Refractive index squared for $s = 0$ (shading) and zonal-mean zonal wind (contour interval of 10 m s^{-1}; thick cyan line represents the zero-wind line) for different runs of the S1 case on the first day of the simulations. (a),(b) Composite of experiments with $\Delta u_m = +10$ and -10 m s^{-1}, respectively; (c),(d) composite of experiments with $\Delta u_m = +5$ and -5 m s^{-1}, respectively; and (e) CTL-S1. The refractive index squared has been nondimensionalized by multiplication by Earth's radius squared.

even for periods longer than 20 days. Insofar as this diagnostic can be interpreted as a measure of the explained variance at given frequencies, this result implies that less than half of the variability of F_z at 100 hPa can be attributed to its variability in the upper troposphere (300 hPa). Figures 15c,d shows the cross spectra of F_z at 100 hPa with all other altitudes and clearly shows a much deeper connection of the flux at 100 hPa with the rest of the stratosphere (squared coherence around 0.6–0.7 at 10 hPa for periods longer than 20 days). These numbers are in fact very similar to those of Polvani and Waugh (2004), who found a linear correlation coefficient of 0.55 between the 40-day-averaged meridional heat flux at 100 and 300 hPa ($0.55^2 = 0.3$, which is within our 0.2–0.4 range). This means the heat flux at 100 hPa is more influenced by other processes (roughly 2/3 of variance explained) than wave injection at 300 hPa (roughly 1/3 of variance explained). We note that even if the 100-hPa fluxes were entirely determined by those at 300 hPa, the coherence between these two levels would not necessarily be close to 1, since a large fraction of the variance at 300 hPa is due to waves that are vertically trapped within the troposphere. However, these results together with the experiments analyzed in section 3 confirm that there is also variance at 100 hPa that is not explained by the 300-hPa fluxes. We finally point out that the fact that the coherence between F_z at 300 and 100 hPa with other stratospheric altitudes ramps up for periods between 10 and 20 days is consistent with the findings that SSWs are associated with wave forcing with time scales longer than 10 days (Sjoberg and Birner 2012).

5. Conclusions

In this paper, we have studied the sensitivity of sudden stratospheric warmings to the stratospheric basic state using the state-of-the-art climate model WACCM4. To isolate stratospheric processes, we have conducted model experiments in which the tropospheric evolution that accompanies selected SSWs is imposed (nudging winds and temperature below 10 km), but the stratosphere is allowed to evolve freely from different initial conditions three weeks before the event in the control runs. This way, the stratospheric control over the evolution of the wave field (and consequently the mean flow) is isolated for the first time in a comprehensive climate model. Our strategy in designing the changes to the initial conditions has been to modify the stratospheric zonal-mean state sufficiently to alter the wave propagation conditions and wave–mean flow interactions. That is why the zonal wind and temperature changes imposed to the initial conditions are zonally symmetric, in gradient wind balance, and of considerable magnitude (the zonal wind has a Gaussian shape in

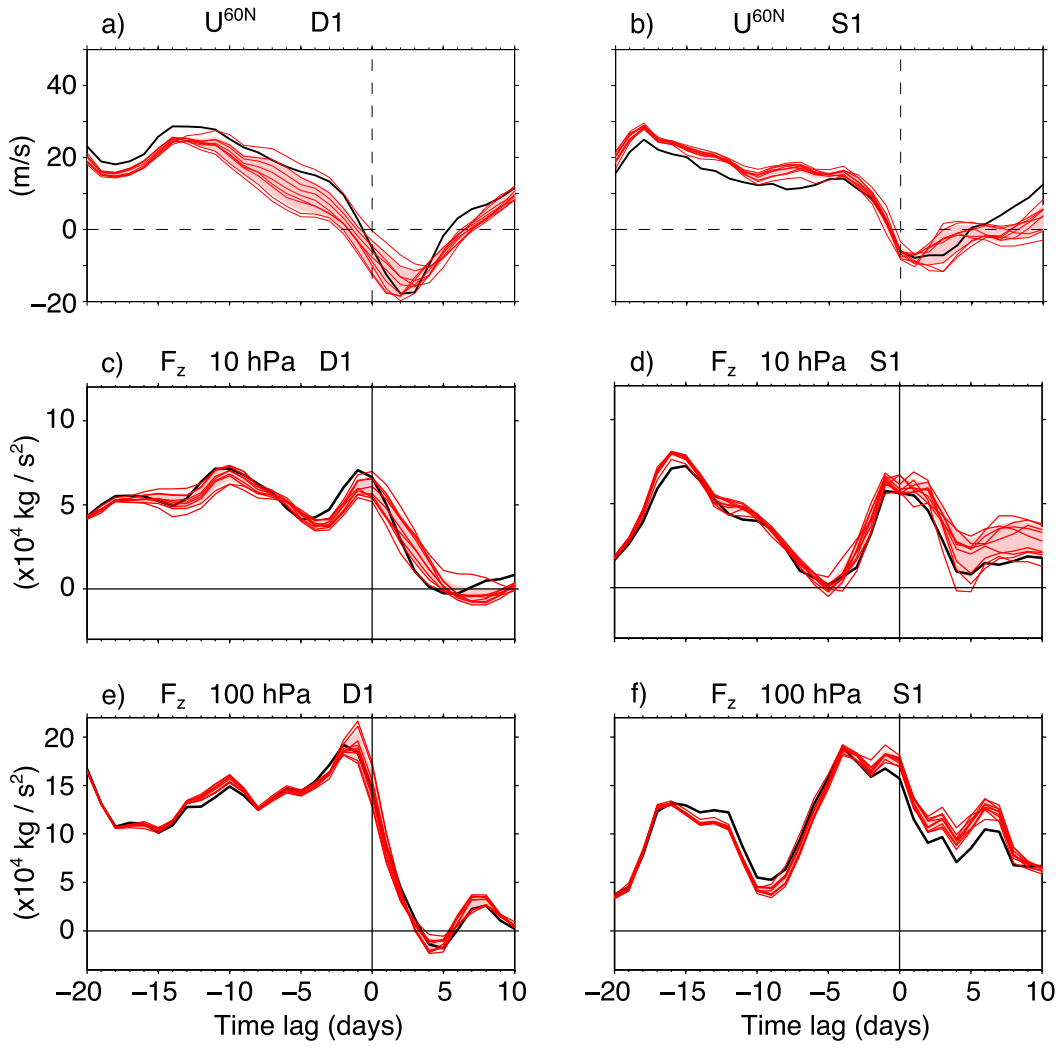

FIG. 14. (top) Zonal-mean zonal wind at 60°N and 10 hPa for (a) CTL-D1 and (b) CTL-S1 (black lines), and the corresponding experiments that do not lead to the SSW when nudging up to 10 km (see Figs. 2b and 6b), but rising the nudging region up to 18 km (red lines). (c)–(f) As in (a) and (b), but showing the corresponding F_z time series at (middle) 10 and (bottom) 100 hPa.

latitude and altitude with a maximum magnitude of $\pm 10\,\mathrm{m\,s^{-1}}$ in a specific location). Because of the characteristics of the tests, with modeled SSWs as targets and constrained tropospheric fields, we have found that such apparently strong initial changes are needed to prevent the SSW from occurring in a significant number of experiments. However, we have shown that those initial changes in the zonal wind and temperature only introduce small alterations to the linear wave propagation conditions as diagnosed by the refractive index squared.

We have performed experiments on six modeled SSWs, and the results demonstrate that the stratospheric flow influences significantly the subsequent development of the SSWs studied. We have analyzed in detail the dynamics in two of the events: one displacement and one split (D1 and S1, respectively). In the case of the displacement event D1, we have found that the different stratospheric initial conditions introduced 21 days before the warming alter the evolution of the wave activity flux F_z (i.e., the vertical component of the EP flux) during the first few days of the model runs, inducing a different stratospheric jet structure that does not lead to a wave amplification and an SSW. In the case of the split event S1, the differences between the experiments with and without a warming are subtler. Both sets of experiments behave similarly during the first 10 days of the simulations. After that time, while the vortex in some experiments evolves toward a highly distorted configuration that eventually splits, the vortex in the other experiments stays coherent for longer times.

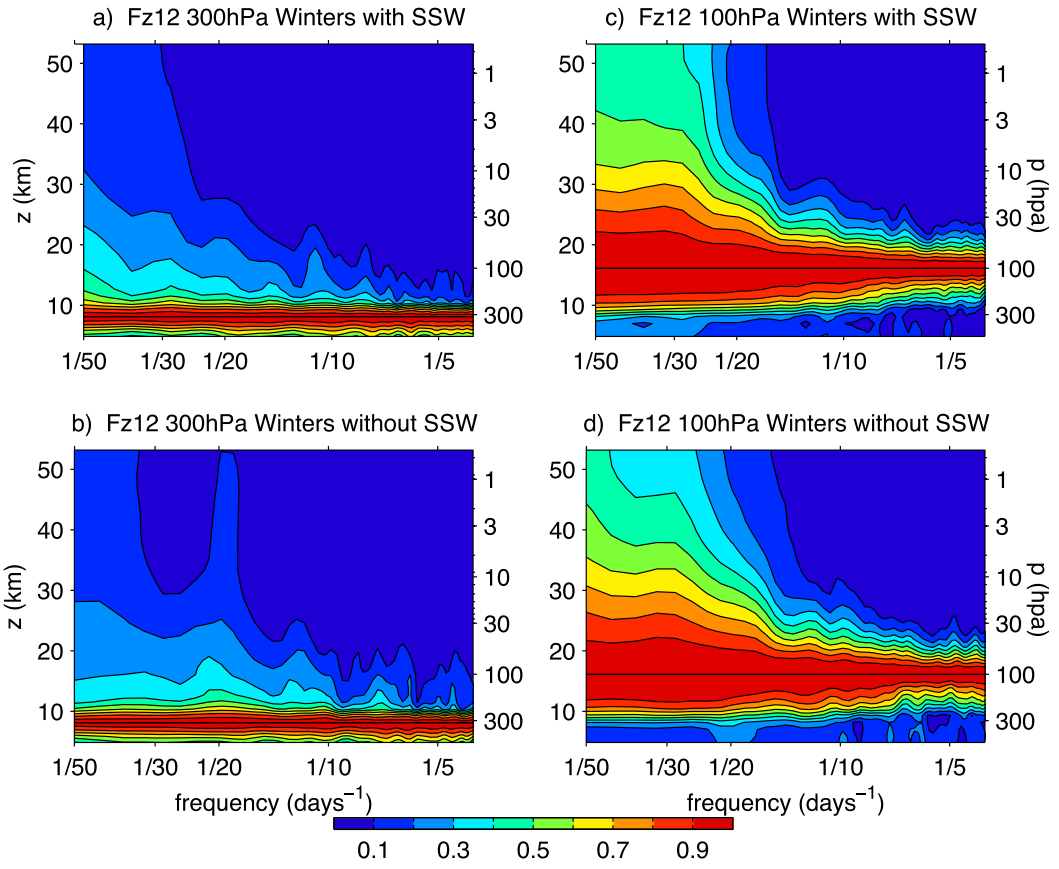

FIG. 15. Coherence squared between the October–March time series of F_z ($s = 1$ and 2) averaged over 45°–75°N at (a),(b) 300 and (c),(d) 100 hPa, and the corresponding time series at all altitudes, for (a),(c) winters with SSW and (b),(d) winters without SSWs.

Another interesting feature is that the vertical evolution of the wave activity is very similar in all the experiments until around 2 days before the warming, when the stratospheric wave-2 activity in the experiments with an SSW experience a sudden growth that induces a much stronger deceleration than in the experiments without a warming. It is clear from the model setup that these differences cannot arise from different tropospheric wave forcing; thus, the state of the stratosphere is playing a dominant role here. We have suggested that differences in the strength of the internal feedback between the stratospheric mean flow and the wave activity flux (Sjoberg and Birner 2014), caused by the different stratospheric mean conditions, may explain the reported differences in stratospheric wave activity flux and the subsequent development of SSWs across experiments.

The outcomes of the other four events studied are consistent with this conclusion and emphasize that the details of how the changes to the initial conditions preclude the SSW are different for each of the six cases. The most striking evidence of this distinct behavior is the fact that in two cases (both of them a split event) only positive initial wind perturbations are effective in preventing the SSW, while in the other four cases (three displacements and one split) only negative initial wind perturbations prevent the warming. Six events are not enough to draw general conclusions in this regard, but it would be interesting to investigate in a future study whether displacement and split events are more sensitive to a particular sign and structures of the initial wind changes, perhaps connected with the different prewarming wind profiles observed for these two types of events (Charlton and Polvani 2007; Albers and Birner 2014).

We have also provided strong evidence pointing out that the use of the meridional heat flux at 100 hPa as a proxy for the tropospheric injection of wave activity into the stratosphere might be misleading. Our results show clearly that key differences arise in this variable at 100 hPa in experiments that do not reproduce the SSW, even though the upper-tropospheric wave activity (at 300 hPa) is practically identical in the experiments that

reproduce and do not reproduce the warming. The fact that the tropospheric upward wave activity is unchanged across the experiments [absence of the external feedback as described by Sjoberg and Birner (2014)] stresses the key role of processes within the stratosphere controlling the wave fluxes at 100 hPa. When the top of the nudging region is placed at 18 km (instead of 10 km), a larger number of experiments develop the SSW in the six cases studied, but not all, which highlights the relevance of stratospheric internal processes for the triggering of these modeled SSW events. In a statistical sense, we have shown that the common variability of the vertical component of the EP flux at 300 hPa (upper troposphere) and 100 hPa (lower stratosphere) is no larger than 20%–40% in the northern winter for periods longer than 20 days; and the common variability of F_z between 300 and 10 hPa is even smaller—about 10%. On the other hand, the common variability of F_z between 100 and 10 hPa goes up to 60%–70%, which partly explains why a larger number of modeled experiments reproduce the sudden warming when the 100-hPa level lies within the nudging altitude range. We conclude that F_z at 100 hPa may be regarded as a symptom but not necessarily a cause of SSWs, consistent with recent studies using mechanistic models and reanalysis data (Jucker 2016; Birner and Albers 2017).

The importance of the stratospheric flow in determining the occurrence of SSW events implies that model biases in the stratospheric winds may be relevant in predictability studies, confirming previous suggestions in this regard (Taguchi 2016; Tripathi et al. 2016; Noguchi et al. 2016). There are also potential implications for seasonal forecasting. For example, one might anticipate that a systematic model drift in forecast models starting from a close-to-observed state, details of parameterized processes such as gravity wave drag (Albers and Birner 2014), or the inclusion of an interactive chemistry model in seasonal forecasting systems, which can alter the stratospheric jet structure through ozone–circulation feedbacks (McCormack et al. 2011; Albers et al. 2013; Cheung et al. 2014), could condition the evolution of the vortex toward (or away from) a configuration that favors the occurrence of a sudden warming.

Acknowledgments. We thank Isla Simpson and two anonymous reviewers for valuable comments that helped improve the manuscript. All data are available upon request to the corresponding author. We acknowledge the use of computational resources (ark:/85065/d7wd3xhc) at the NCAR-Wyoming Supercomputing Center provided by the National Science Foundation and the State of Wyoming and supported by NCAR's Computational and Information Systems Laboratory. AdlC is supported by the Advanced Study Program at NCAR. The National Center for Atmospheric Research is sponsored by the National Science Foundation.

REFERENCES

Albers, J. R., and T. Birner, 2014: Vortex preconditioning due to planetary and gravity waves prior to sudden stratospheric warmings. *J. Atmos. Sci.*, **71**, 4028–4054, doi:10.1175/JAS-D-14-0026.1.

——, J. P. McCormack, and T. R. Nathan, 2013: Stratospheric ozone and the morphology of the northern hemisphere planetary waveguide. *J. Geophys. Res. Atmos.*, **118**, 563–576, doi:10.1029/2012JD017937.

——, G. N. Kiladis, T. Birner, and J. Dias, 2016: Tropical upper-tropospheric potential vorticity intrusions during sudden stratospheric warmings. *J. Atmos. Sci.*, **73**, 2361–2384, doi:10.1175/JAS-D-15-0238.1.

Attard, H. E., R. Rios-Berrios, C. T. Guastini, and A. L. Lang, 2016: Tropospheric and stratospheric precursors to the January 2013 sudden stratospheric warming. *Mon. Wea. Rev.*, **144**, 1321–1339, doi:10.1175/MWR-D-15-0175.1.

Ayarzagüena, B., U. Langematz, and E. Serrano, 2011: Tropospheric forcing of the stratosphere: A comparative study of the two different major stratospheric warmings in 2009 and 2010. *J. Geophys. Res.*, **116**, D18114, doi:10.1029/2010JD015023.

Baldwin, M. P., and T. J. Dunkerton, 2001: Stratospheric harbingers of anomalous weather regimes. *Science*, **294**, 581–584, doi:10.1126/science.1063315.

Barriopedro, D., and N. Calvo, 2014: On the relationship between ENSO, stratospheric sudden warmings, and blocking. *J. Climate*, **27**, 4704–4720, doi:10.1175/JCLI-D-13-00770.1.

Birner, T., and J. R. Albers, 2017: Sudden stratospheric warmings and anomalous upward wave activity flux. *SOLA*, **13A**, 8–12, doi:10.2151/sola.13A-002.

Butler, A. H., and L. M. Polvani, 2011: El Niño, La Niña, and stratospheric sudden warmings: A reevaluation in light of the observational record. *Geophys. Res. Lett.*, **38**, L13807, doi:10.1029/2011GL048084.

——, D. J. Seidel, S. C. Hardiman, N. Butchart, T. Birner, and A. Match, 2015: Defining sudden stratospheric warmings. *Bull. Amer. Meteor. Soc.*, **96**, 1913–1928, doi:10.1175/BAMS-D-13-00173.1.

Charlton, A. J., and L. M. Polvani, 2007: A new look at stratospheric sudden warmings. Part I: Climatology and modeling benchmarks. *J. Climate*, **20**, 449–469, doi:10.1175/JCLI3996.1.

Chen, P., and W. A. Robinson, 1992: Propagation of planetary waves between the troposphere and stratosphere. *J. Atmos. Sci.*, **49**, 2533–2545, doi:10.1175/1520-0469(1992)049<2533:POPWBT>2.0.CO;2.

Cheung, J. C. H., J. D. Haigh, and D. R. Jackson, 2014: Impact of EOS MLS ozone data on medium-extended range ensemble weather forecasts. *J. Geophys. Res. Atmos.*, **119**, 9253–9266, doi:10.1002/2014JD021823.

Christiansen, B., 1999: Stratospheric vacillations in a general circulation model. *J. Atmos. Sci.*, **56**, 1858–1872, doi:10.1175/1520-0469(1999)056<1858:SVIAGC>2.0.CO;2.

Clark, J. H. E., 1974: Atmospheric response to the quasi-resonant of forced planetary waves. *J. Meteor. Soc. Japan*, **52**, 143–162, doi:10.2151/jmsj1965.52.1_143.

Díaz-Durán, A., E. Serrano, B. Ayarzagüena, M. Abalos, and A. de la Cámara, 2017: Intra-seasonal variability of extreme boreal stratospheric polar vortex events and their precursors. *Climate Dyn.*, doi:10.1007/s00382-017-3524-1.

Esler, J. G., and R. K. Scott, 2005: Excitation of transient Rossby waves on the stratospheric polar vortex and the barotropic sudden warming. *J. Atmos. Sci.*, **62**, 3661–3682, doi:10.1175/JAS3557.1.

——, and N. J. Matthewman, 2011: Stratospheric sudden warmings as self-tuning resonances. Part II: Vortex displacement events. *J. Atmos. Sci.*, **68**, 2505–2523, doi:10.1175/JAS-D-11-08.1.

Garcia, R. R., D. R. Marsh, D. E. Kinnison, B. A. Boville, and F. Sassi, 2007: Simulation of secular trends in the middle atmosphere, 1950–2003. *J. Geophys. Res.*, **112**, D09301, doi:10.1029/2006JD007485.

——, A. K. Smith, D. E. Kinnison, Á. de la Cámara, and D. J. Murphy, 2017: Modification of the gravity wave parameterization in the Whole Atmosphere Community Climate Model: Motivation and results. *J. Atmos. Sci.*, **74**, 275–291, doi:10.1175/JAS-D-16-0104.1.

Geisler, J. E., 1974: Numerical model of sudden stratospheric warming mechanism. *J. Geophys. Res.*, **79**, 4989–4999, doi:10.1029/JC079i033p04989.

Gómez-Escolar, M., N. Calvo, D. Barriopedro, and S. Fueglistaler, 2014: Tropical response to stratospheric sudden warmings and its modulation by the QBO. *J. Geophys. Res. Atmos.*, **119**, 7382–7395, doi:10.1002/2013JD020560.

Harnik, N., 2009: Observed stratospheric downward reflection and its relation to upward pulses of wave activity. *J. Geophys. Res.*, **114**, D08120, doi:10.1029/2008JD010493.

Hitchcock, P., and P. H. Haynes, 2016: Stratospheric control of planetary waves. *Geophys. Res. Lett.*, **43**, 11 884–11 892, doi:10.1002/2016GL071372.

——, and I. R. Simpson, 2016: Quantifying eddy feedbacks and forcings in the tropospheric response to stratospheric sudden warmings. *J. Atmos. Sci.*, **73**, 3641–3657, doi:10.1175/JAS-D-16-0056.1.

Holt, L. A., C. E. Randall, E. D. Peck, D. R. Marsh, A. K. Smith, and V. L. Harvey, 2013: The influence of major sudden stratospheric warming and elevated stratopause events on the effects of energetic particle precipitation in WACCM. *J. Geophys. Res. Atmos.*, **118**, 11 636–11 646, doi:10.1002/2013JD020294.

Holton, J. R., and C. Mass, 1976: Stratospheric vacillation cycles. *J. Atmos. Sci.*, **33**, 2218–2225, doi:10.1175/1520-0469(1976)033<2218:SVC>2.0.CO;2.

Ineson, S., and A. Scaife, 2009: The role of the stratosphere in the European climate response to El Niño. *Nat. Geosci.*, **2**, 32–36, doi:10.1038/ngeo381.

Jucker, M., 2016: Are sudden stratospheric warmings generic? Insights from an idealized GCM. *J. Atmos. Sci.*, **73**, 5061–5080, doi:10.1175/JAS-D-15-0353.1.

Kolstad, E. W., S. P. Sobolowski, and A. A. Scaife, 2015: Intra-seasonal persistence of European surface temperatures. *J. Climate*, **28**, 5365–5374, doi:10.1175/JCLI-D-15-0053.1.

Limpasuvan, V., D. W. J. Thompson, and D. L. Hartmann, 2004: The life cycle of the Northern Hemisphere sudden stratospheric warmings. *J. Climate*, **17**, 2584–2596, doi:10.1175/1520-0442(2004)017<2584:TLCOTN>2.0.CO;2.

Liu, C., B. Tian, K.-F. Li, G. L. Manney, N. J. Livesey, Y. L. Yung, and D. E. Waliser, 2014: Northern Hemisphere mid-winter vortex-displacement and vortex-split stratospheric sudden warmings: Influence of the Madden-Julian Oscillation and Quasi-Biennial Oscillation. *J. Geophys. Res. Atmos.*, **119**, 12 599–12 620, doi:10.1002/2014JD021876.

Manney, G. L., Z. D. Lawrence, M. L. Santee, N. J. Livesey, A. Lambert, and M. C. Pitts, 2015: Polar processing in a split vortex: Arctic ozone loss in early winter 2012/2013. *Atmos. Chem. Phys.*, **15**, 5381–5403, doi:10.5194/acp-15-5381-2015.

Marsh, D. R., M. J. Mills, D. E. Kinnison, J.-F. Lamarque, N. Calvo, and L. M. Polvani, 2013: Climate change from 1850 to 2005 simulated in CESM1(WACCM). *J. Climate*, **26**, 7372–7391, doi:10.1175/JCLI-D-12-00558.1.

Marshall, A. G., and A. A. Scaife, 2010: Improved predictability of stratospheric sudden warming events in an atmospheric general circulation model with enhanced stratospheric resolution. *J. Geophys. Res.*, **115**, D16114, doi:10.1029/2009JD012643.

Martius, O., L. M. Polvani, and H. C. Davies, 2009: Blocking precursors to stratospheric sudden warming events. *Geophys. Res. Lett.*, **36**, L14806, doi:10.1029/2009GL038776.

Matsuno, T., 1970: Vertical propagation of stationary planetary waves in the winter Northern Hemisphere. *J. Atmos. Sci.*, **27**, 871–883, doi:10.1175/1520-0469(1970)027<0871:VPOSPW>2.0.CO;2.

——, 1971: A dynamical model of the stratospheric sudden warming. *J. Atmos. Sci.*, **28**, 1479–1494, doi:10.1175/1520-0469(1971)028<1479:ADMOTS>2.0.CO;2.

Matthewman, N. J., and J. G. Esler, 2011: Stratospheric sudden warmings as self-tuning resonances. Part I: Vortex splitting events. *J. Atmos. Sci.*, **68**, 2481–2504, doi:10.1175/JAS-D-11-07.1.

McCormack, J. P., T. R. Nathan, and E. C. Cordero, 2011: The effect of zonally asymmetric ozone heating on the Northern Hemisphere winter polar stratosphere. *Geophys. Res. Lett.*, **38**, L03802, doi:10.1029/2010GL045937.

McIntyre, M. E., 1982: How well do we understand the dynamics of stratospheric warmings? *J. Meteor. Soc. Japan*, **60**, 37–65, doi:10.2151/jmsj1965.60.1_37.

Müller, R., and G. Günther, 2003: A generalized form of Lait's modified potential vorticity. *J. Atmos. Sci.*, **60**, 2229–2237, doi:10.1175/1520-0469(2003)060<2229:AGFOLM>2.0.CO;2.

Nishii, K., H. Nakamura, and T. Miyasaka, 2009: Modulations in the planetary wave field induced by upward-propagating Rossby wave packets prior to stratospheric sudden warming events: A case-study. *Quart. J. Roy. Meteor. Soc.*, **135**, 39–52, doi:10.1002/qj.359.

Noguchi, S., H. Mukougawa, Y. Kuroda, R. Mizuta, S. Yabu, and H. Yoshimura, 2016: Predictability of the stratospheric polar vortex breakdown: An ensemble reforecast experiment for the splitting event in January 2009. *J. Geophys. Res. Atmos.*, **121**, 3388–3404, doi:10.1002/2015JD024581.

Plumb, R. A., 1981: Instability of the distorted polar night vortex: A theory of stratospheric warmings. *J. Atmos. Sci.*, **38**, 2514–2531, doi:10.1175/1520-0469(1981)038<2514:IOTDPN>2.0.CO;2.

Polvani, L. M., and D. W. Waugh, 2004: Upward wave activity flux as a precursor to extreme stratospheric events and subsequent anomalous surface weather regimes. *J. Climate*, **17**, 3548–3554, doi:10.1175/1520-0442(2004)017<3548:UWAFAA>2.0.CO;2.

Rayner, N. A., D. E. Parker, E. B. Horton, C. K. Folland, L. V. Alexander, D. P. Rowell, E. C. Kent, and A. Kaplan, 2003: Global analyses of sea surface temperature, sea ice, and night marine air temperature since the late nineteenth century. *J. Geophys. Res.*, **108**, 4407, doi:10.1029/2002JD002670.

Scaife, A. A., and Coauthors, 2016: Seasonal winter forecasts and the stratosphere. *Atmos. Sci. Lett.*, **17**, 51–56, doi:10.1002/asl.598.

Schneidereit, A., and Coauthors, 2017: Enhanced tropospheric wave forcing of two anticyclones in the prephase of January 2009 major stratospheric sudden warming event. *Mon. Wea. Rev.*, **145**, 1797–1815, doi:10.1175/MWR-D-16-0242.1.

Scott, R. K., and L. M. Polvani, 2004: Stratospheric control of upward wave flux near the tropopause. *Geophys. Res. Lett.*, **31**, L02115, doi:10.1029/2003GL017965.

——, and ——, 2006: Internal variability of the winter stratosphere. Part I: Time-independent forcing. *J. Atmos. Sci.*, **63**, 2758–2776, doi:10.1175/JAS3797.1.

Sigmond, M., J. F. Scinocca, V. V. Kharin, and T. G. Shepherd, 2013: Enhanced seasonal forecast skill following stratospheric sudden warmings. *Nat. Geosci.*, **6**, 98–102, doi:10.1038/ngeo1698.

Sjoberg, J. P., and T. Birner, 2012: Transient tropospheric forcing of sudden stratospheric warmings. *J. Atmos. Sci.*, **69**, 3420–3432, doi:10.1175/JAS-D-11-0195.1.

——, and ——, 2014: Stratospheric wave–mean flow feedbacks and sudden stratospheric warmings in a simple model forced by upward wave activity flux. *J. Atmos. Sci.*, **71**, 4055–4071, doi:10.1175/JAS-D-14-0113.1.

Smith, A. K., 1989: An investigation of resonant waves in a numerical model of an observed sudden stratospheric warming. *J. Atmos. Sci.*, **46**, 3038–3054, doi:10.1175/1520-0469(1989)046<3038:AIORWI>2.0.CO;2.

——, 1992: Preconditioning for stratospheric sudden warmings: Sensitivity studies with a numerical model. *J. Atmos. Sci.*, **49**, 1003–1019, doi:10.1175/1520-0469(1992)049<1003:PFSSWS>2.0.CO;2.

——, N. M. Pedatella, D. R. Marsh, and T. Matsuo, 2017: On the dynamical control of the mesosphere–lower thermosphere by the lower and middle atmosphere. *J. Atmos. Sci.*, **74**, 933–947, doi:10.1175/JAS-D-16-0226.1.

Solomon, S., D. Kinnison, J. Bandoro, and R. Garcia, 2015: Simulation of polar ozone depletion: An update. *J. Geophys. Res. Atmos.*, **120**, 7958–7974, doi:10.1002/2015JD023365.

Sun, L., W. A. Robinson, and G. Chen, 2012: The predictability of stratospheric warming events: More from the troposphere or the stratosphere? *J. Atmos. Sci.*, **69**, 768–783, doi:10.1175/JAS-D-11-0144.1.

Taguchi, M., 2014: Predictability of major stratospheric sudden warmings of the vortex split type: Case study of the 2002 southern event and the 2009 and 1989 northern events. *J. Atmos. Sci.*, **71**, 2886–2904, doi:10.1175/JAS-D-13-078.1.

——, 2016: Connection of predictability of major stratospheric sudden warmings to polar vortex geometry. *Atmos. Sci. Lett.*, **17**, 33–38, doi:10.1002/asl.595.

Thompson, D. W. J., M. P. Baldwin, and J. M. Wallace, 2002: Stratospheric connection to Northern Hemisphere wintertime weather: Implications for prediction. *J. Climate*, **15**, 1421–1428, doi:10.1175/1520-0442(2002)015<1421:SCTNHW>2.0.CO;2.

Tripathi, O. P., and Coauthors, 2015: The predictability of the extratropical stratosphere on monthly time-scales and its impact on the skill of tropospheric forecasts. *Quart. J. Roy. Meteor. Soc.*, **141**, 987–1003, doi:10.1002/qj.2432.

——, and Coauthors, 2016: Examining the predictability of the stratospheric sudden warming of January 2013 using multiple NWP systems. *Mon. Wea. Rev.*, **144**, 1935–1960, doi:10.1175/MWR-D-15-0010.1.

Tung, K. K., and R. S. Lindzen, 1979: A theory of stationary long waves. Part II: Resonant Rossby waves in the presence of realistic vertical shears. *Mon. Wea. Rev.*, **107**, 735–750, doi:10.1175/1520-0493(1979)107<0735:ATOSLW>2.0.CO;2.

von Storch, H., and F. W. Zwiers, 1999: *Statistical Analysis in Climate Research.* Cambridge University Press, 484 pp.

Woollings, T., A. Charlton-Perez, S. Ineson, A. G. Marshall, and G. Masato, 2010: Associations between stratospheric variability and tropospheric blocking. *J. Geophys. Res.*, **115**, D06108, doi:10.1029/2009JD012742.